

# LOAN DOCUMENT

PHOTOGRAPH THIS SHEET

AD-A239 092



DTIC ACCESSION NUMBER

LEVEL

INVENTORY

WL-TR-91-3057

DOCUMENT IDENTIFICATION

Jul 1991

DISTRIBUTION STATEMENT

ACCESSION FOR

NTIS GRA&I  
DTIC TRAC  
UNANNOUNCED  
JUSTIFICATION



BY

DISTRIBUTION/

AVAILABILITY CODES

DISTRIBUTION

AVAILABILITY AND/OR SPECIAL

A-1

DISTRIBUTION STAMP

DATE ACCESSIONED

DATE RETURNED

91 7 1 025

91-06600



DATE RECEIVED IN DTIC

REGISTERED OR CERTIFIED NUMBER

PHOTOGRAPH THIS SHEET AND RETURN TO DTIC-FDAC

H  
A  
N  
D  
L  
E  
  
W  
I  
T  
H  
  
C  
A  
R  
E

**AD-A239 092**

WL-TR-91-3057



**FLUCTUATING PRESSURE LOADS FOR  
HYPERSONIC VEHICLE STRUCTURES**



**H. G. Lew  
Tech Quest Inc.  
3315 Bob Wallace Avenue  
Huntsville, AL 35805**

**and**

**A. L. Laganelli  
Science Applications Int'l Corp.  
501 Office Center Drive, Suite 420  
Ft. Washington, PA 19034**

July 1991

**FINAL REPORT FOR PERIOD: 10 AUGUST 1990 - 10 FEBRUARY 1991**

**Approved for Public Release, distribution Unlimited**

FLIGHT DYNAMICS DIRECTORATE  
WRIGHT LABORATORY  
AIR FORCE SYSTEMS COMMAND  
WRIGHT-PATTERSON AIR FORCE BASE, OHIO 45433-6553

# REPORT DOCUMENTATION PAGE

Form Approved  
OMB No. 0704-0188

Public reporting burden for this collection of information is estimated to average 1 hour per response, including the time for reviewing instructions, searching existing data sources, gathering and maintaining the data needed, and completing and reviewing the collection of information. Send comments regarding this burden estimate or any other aspect of this collection of information, including suggestions for reducing this burden, to Washington Headquarters Services, Directorate for Information Operations and Reports, 1215 Jefferson Davis Highway, Suite 1204, Arlington, VA 22202-4302, and to the Office of Management and Budget, Paperwork Reduction Project (0704-0188), Washington, DC 20503.

|   |   |  |                                  |  |  |
|---|---|--|----------------------------------|--|--|
| 1. AGENCY USE ONLY (Leave blank)  |   | 2. REPORT DATE<br>July 1991                                |                                  | 3. REPORT TYPE AND DATES COVERED<br>FINAL: 10 Aug 90 - 10 Feb 91                               |  |
| 4. TITLE AND SUBTITLE<br>Fluctuating Pressure Loads for Hypersonic Vehicle Structures   |   |  |                                  | 5. FUNDING NUMBERS<br>Contract:<br>F33615-90-C- 3210<br>PE 65502F<br>PR 3005<br>TA 40<br>WU 84 |  |
| 6. AUTHOR(S)<br>Henry G. Lew and Anthony L. Laganelli   |   |  |                                  |  |  |
| 7. PERFORMING ORGANIZATION NAME(S) AND ADDRESS(ES)<br>TechQuest, Inc.<br>3315 Bob Wallace Avenue<br>Huntsville, AL 35805  |   |  |                                  | 8. PERFORMING ORGANIZATION<br>REPORT NUMBER<br><br>TQ-TR-91-01                                 |  |
| 9. SPONSORING / MONITORING AGENCY NAME(S) AND ADDRESS(ES)<br>Leonard Shaw (513) 255-5229<br>Flight Dynamics Directorate (WL/FIBG)<br>Wright Laboratory<br>Wright-Patterson Air Force Base, Ohio 45433-6553  |   |  |                                  | 10. SPONSORING / MONITORING<br>AGENCY REPORT NUMBER<br><br>WL-TR-91-3057                       |  |
| 11. SUPPLEMENTARY NOTES<br><br>Report prepared as SBIR Phase I (AF90-101) with Science Applications International Corpora-<br>tion as a subcontractor.  |   |  |                                  |  |  |
| 12a. DISTRIBUTION / AVAILABILITY STATEMENT<br><br>Approved for public release; distribution is unlimited.   |   |  |                                  | 12b. DISTRIBUTION CODE   |  |
| 13. ABSTRACT (Maximum 200 words)<br><br>An SBIR Phase I investigation was conducted to determine the ability to predict acoustic loads on supersonic/hypersonic structures with attached and separated flows. These techniques, which are based on laws governing boundary layer flow and shock physics, provide scaling parameters to extrapolate ground test results to flight conditions and can be used for the design process. It was determined that efficient, thin aerodynamic control surfaces generally produce weak shock/boundary layers interactions where the rms pressure levels are not significantly augmented over attached flow levels. The exception to these findings include: 1) corner flow (inlet and stabilizers), 2) bow shock interaction (inlet and stabilizer), and 3) shock on shock/boundary layer (cowl/inlet, bow shock/inlet, and bow/inlet/cowl). Other potential interactions that may cause problems have been identified as: 1) axial offset (non-common intersection of two planes), 2) shock interaction with laminar boundary layers, 3) angle of attack effects, and 4) viscous approach flow along ramp leading to the inlet. An experimental program is recommended to address these issues; in particular for $M > 3$ where acoustic data does not exist. These experiments should be conducted in a facility that allows for preliminary test runs to ensure desired results. The WRDC Mach 3 and Mach 12 facilities are recommended for a Phase II investigation. The results of the Phase I and Phase II effort will provide the Air Force with the ability to design structures subject to complex flow interactions such as the National AeroSpace Plane. |   |  |                                  |  |  |
| 14. SUBJECT TERMS<br><br>Fluctuating Pressure, Prediction, Hypersonic, Structures   |   |  |                                  | 15. NUMBER OF PAGES<br>75  |  |
|   |   |  |                                  | 16. PRICE CODE   |  |
| 17. SECURITY CLASSIFICATION<br>OF REPORT<br>UNCLASSIFIED  | 18. SECURITY CLASSIFICATION<br>OF THIS PAGE<br>UNCLASSIFIED | 19. SECURITY CLASSIFICATION<br>OF ABSTRACT<br>UNCLASSIFIED | 20. LIMITATION OF ABSTRACT<br>UL |  |  |

# NOTICE

When Government drawings, specifications, or other data are used for any purpose other than in connection with a definitely Government-related procurement, the United States Government incurs no responsibility or any obligation whatsoever. The fact that the government may have formulated or in any way supplied the said drawings, specifications, or other data, is not to be regarded by implication, or otherwise in any manner construed, as licensing the holder, or any other person or corporation; or as conveying any rights or permission to manufacture, use, or sell any patented invention that may in any way be related thereto.

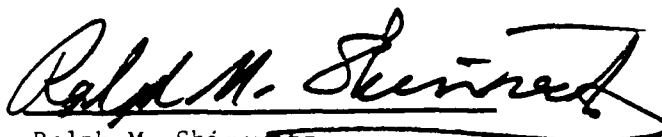
This report is releasable to the National Technical Information Service (NTIS). At NTIS, it will be available to the general public, including foreign nations.

This technical report has been reviewed and is approved for publication.



Leonard L. Shaw  
Aerospace Engineer  
Acoustics and Sonic Fatigue

FOR THE COMMANDER



Ralph M. Shimovetz  
Technical Manager  
Acoustics and Sonic Fatigue



Jerome Pearson, Chief  
Structural Dynamics Branch  
Structures Division

If your address has changed, if you wish to be removed from our mailing list, or if the addressee is no longer employed by your organization please notify WL/FIBG, WPAFB, OH 45433-6553 to help us maintain a current mailing list.

Copies of this report should not be returned unless return is required by security considerations, contractual obligations, or notice on a specific document.

# TABLE OF CONTENTS

| SECTION   | PAGE |
|---|------|
| TABLE OF CONTENTS   | i    |
| LIST OF FIGURES   | iii  |
| NOMENCLATURE  | v    |
| I. INTRODUCTION AND SIGNIFICANCE OF THE PROBLEM                   | 1    |
| II. AEROACOUSTIC LOAD PREDICTION                                  | 2    |
| 1. Attached Flow-Smooth and Rough Surfaces                        | 2    |
| a. Smooth surfaces  | 2    |
| * Power Spectra   | 6    |
| * Cross-Power Spectra   | 7    |
| b. Rough Surface  | 9    |
| 2. Separated Flows  | 9    |
| 3. Shock Wave/Boundary Layer Interaction<br>(non-attached)        | 10   |
| a. 2D compression corner  | 10   |
| b. 3D swept-fin   | 12   |
| c. Correlation of rms Pressure and<br>Power Spectra               | 14   |
| * 3D Shock Wave/Boundary Interactions                             |      |
| * Power Spectra   |      |
| 4. Application to McDonnell-Douglas Blended<br>Wing Body          | 22   |
| a. BWB Flowfield  | 22   |
| b. BWB Acoustic Loads-Attached Turbulent<br>Boundary Flow         | 24   |
| c. BWB Acoustic Loads-Shock/Boundary<br>Layer Interaction Regions | 26   |
| 5. Assessment of Literature Review and<br>Prediction Capability   | 33   |

| SECTION  | PAGE |
|--|------|
| III. EVALUATION OF ATTACHED AND SEPARATED FLOW<br>EXPERIMENTS AT MACH 4 AND MACH 8 | 35   |
| 1. AEDC Mach 4 and Mach 8 Data   | 35   |
| 2. Assessment of the AEDC Mach 4 and Mach 8<br>Data Base                           | 40   |
| IV. EXPERIMENTAL PLAN  | 51   |
| 1. Introduction/Problem Definition   | 51   |
| 2. Purpose and Objective of Wind Tunnel<br>Program                                 | 53   |
| 3. Test Hardware   | 54   |
| 3.1 Test Model   | 54   |
| 4. Instrumentation   | 56   |
| 5. Test Matrix   | 57   |
| V. ASSESSMENT OF PHASE I PROGRAM AND RECOMMENDATIONS<br>FOR PHASE II - EFFORT      | 60   |
| 1. Assessment of Phase I Program   | 60   |
| 2. Recommendations for Phase II - Effort   | 62   |
| VI. REFERENCES   | 63   |

| LIST OF FIGURES   | PAGE |
|---|------|
| 1. Hypersonic Space Transportation System with Flow Interaction Regimes.  | 3    |
| 2. RMS Pressure Variation with Mach Number - Attached Turbulent Boundary Layer Flow (Smooth Wall) References 1 and 2          | 6    |
| 3. Comparison of Normalized Spectral Measurements (Reference 1) and Theory.   | 8    |
| 4. Typical Example of Compression Corner Shock/ Boundary Layer Interaction (24° Ramp) - Reference 14                          | 11   |
| 5. RMS Pressure Distribution with Shock Strength (2D Interaction) - Reference (13).   | 13   |
| 6. Fin Generated (3D) Shock/Boundary Layer Interactions for Mean (A) and Fluctuating (B) Pressure - References (19) and (20). | 13   |
| 7. Peak rms Pressure Variations for 2D/3D Interaction with Shock Strength - Reference (17).                                   | 15   |
| 8. Correlation of Peak rms Pressure for Shock/Boundary Layer Interactions   | 19   |
| 9. Comparison of Prediction Technique to Measured Power Spectral Density Data for a 24° Compression Ramp                      | 20   |
| 10. Comparison of Prediction Technique to Measured Power Spectral Data for a 20° Fin Shock Generator                          | 20   |
| 11. Blended Wing Body Investigation Regions Model   | 23   |
| 12. Boundary Layer Properties Generated for 3% BWB Using 3D Parabolized Navier-Stokes Solution                                | 25   |
| 13. RMS Pressure Distribution on Leeward and Windward Meridians of BWB Configurations at Mach 10                              | 27   |
| 14. Power Spectra on Windward Meridian of BWB at Mach 10  | 28   |
| 15. Power Spectra on Leeward Meridian of BWB at Mach 10   | 29   |
| 16. Views of Blended Wing Body (a-d) and Potential Shock/Boundary Layer Interactions (e-h).                                   | 31   |
| 17. MaRV Wind Tunnel Models - Tested at AEDC  | 36   |

| LIST OF FIGURES (continued)   | PAGE |
|---|------|
| 18. RMS Pressure Distribution with Local Surface Pressure at Mach 4           | 38   |
| 19. RMS Pressure Distribution with Local Surface Pressure at Mach 8           | 39   |
| 20. Typical Cone-Slice-Flap Configuration with Streamline Spreading           | 42   |
| 21. PNS Solution for Pressure Contours on Blunt Cone with 15° Flap at Mach 4. | 44   |
| 22. PNS Solution for Pressure Contours on Blunt Cone with 15° Flap at Mach 8. | 47   |
| 23. Inviscid Interactions of Boundary Layer with Compression Corner           | 50   |
| 24. WRDC Mach 3 Facility Test Model   | 55   |
| 25. WRDC Mach 12 Facility Test Model  | 59   |



## NOMENCLATURE

|                          |  |
|--------------------------|--|
| $b$                      | Compressibility exponent - Eq. (4)                                 |
| $C_p, \overline{C_p}$    | Pressure coefficient - $(P-P_1)/q_1$                               |
| $C_f$                    | Skin-friction coefficient  |
| $f, \omega$              | Frequency  |
| $F_C$                    | Compressible/incompressible transformation functions - Eq. (3)     |
| $h$                      | Enthalpy   |
| $k'$                     | Parameter defined in Eqs. (6), $F_C^{-2\lambda}$                   |
| $K$                      | Parameter defined in Eq. (5)                                       |
| $l$                      | Characteristic length  |
| $M$                      | Mach number  |
| $\tilde{p}, p_{rms}, p'$ | rms fluctuating pressure   |
| $p_w, \overline{p_w}$    | Local boundary layer static pressure                               |
| $q$                      | Dynamic pressure $((\gamma/2) \rho M^2)$                           |
| $r$                      | Recovery factor (0.896 for turbulent flow)                         |
| $Re$                     | Reynolds number  |
| $St$                     | Stanton number   |
| $t$                      | Time   |
| $u, v$                   | Velocity in stream directions, normal direction                    |
| $V$                      | Characteristic velocity  |
| $x, y$                   | Coordinate distance in stream and spanwise direction, respectively |

### Greek Symbols

|                            |  |
|----------------------------|--|
| $\alpha$                   | Shock generator angle, angle of attack                                 |
| $\beta$                    | Correction to swept shock - Eq. (11)                                   |
| $\gamma$                   | Ratio of specific heats (1.4 for air)                                  |
| $\delta, \delta^*, \theta$ | Boundary layer displacement, and momentum thicknesses                  |
| $\theta_s$                 | Oblique shock angle  |
| $\lambda$                  | Parameter, viscous/velocity power law exponents $[2m-(1+n)]/(3+n)$     |
| $\tau$                     | Shear stress   |
| $\phi$                     | Shock angle based on swept shock/boundary layer interaction - Eq. (11) |
| $\phi(\omega), \phi(f)$    | Power spectral density   |

### Subscripts

|          |   |
|----------|---|
| 0        | Reference condition (smooth or upstream of interaction) |
| 1        | Approach flow-upstream of interaction                   |
| 2        | Shock/boundary layer interaction region (peak, plateau) |
| aw       | Adiabatic wall  |
| c        | Compressible conditions                                 |
| e        | Evaluated at edge of boundary layer                     |
| i        | Incompressible conditions                               |
| x        | Based on wetted length, axial length                    |
| w        | Wall  |
| $\infty$ | Freestream conditions                                   |

### Superscript

|   |   |
|---|---|
| * | Based on reference temperature conditions |
|---|---|

### Acronyms

|     |                             |
|-----|-----------------------------|
| BWB | Blended Wing Body           |
| HS  | Horizontal Stabilizer       |
| VS  | Vertical Stabilizer         |
| STS | Space Transportation System |
| PNS | Parabolized Navier Stokes   |
| PSD | Power Spectral Density      |
| LBL | Laminar Boundary Layer      |
| TBL | Turbulent Boundary Layer    |
| TPS | Thermal Protection System   |

## I. INTRODUCTION AND SIGNIFICANCE OF THE PROBLEM

Hypersonic vehicles in flight are subjected to critical loads which have increased the complexity of their structural design. One of the most critical ones is the high temperature environment. A second one is the effect of the fluctuating pressure generated by the hypersonic turbulent boundary layer and its interaction with the accompanying shock wave system especially those from lifting surfaces. These two effects have a strong impact on the structural response of the vehicle and must be factored into the vehicle design.

In addition to causing potential structural failure, the turbulent induced aeroacoustic excitations can cause unacceptable sound pressure levels to equipment stations on the vehicle as well as the crew compartment in manned vehicles. Hypersonic vehicle structures featuring control surfaces can generate significant sound pressure levels as a result of the increased static pressure levels and is a potential for separated flow regions. Thus, in order to perform a structural fatigue analysis of a vehicle in this environment the requirement is the prediction of the aeroacoustic loads for the flowfield behavior as dictated by the mission of the vehicle.

The prediction of aeroacoustic loads on hypersonic structures have used empirical models based on ground test data and limited flight data for axisymmetric as well as 3D maneuvering bodies as given in References (1 and 2). Both ground and flight measurements show high vibration levels that were attributed to flow interactions associated with control surfaces.

The algorithms that have been developed for hypersonic flow conditions are generally for shapes that are planar, 2D, or axisymmetric except for control surface regions. Moreover, the

algorithms which were based on physical laws, are generally for attached boundary turbulent boundary layer flows. Regions experiencing flow separation have a complex flow structure and present a more difficult problem for modeling. Future hypersonic vehicles will require lifting body configurations where vehicle lengths can be an order of magnitude longer than those configurations from which present aeroacoustic predictive techniques were developed. A typical hypersonic configuration featuring 3D non-circular cross-sections with ramps, control surfaces, and shock/boundary layer interactions is shown in Figure (1).

This document will review the analytical and experimental works to date on the prediction of aeroacoustics loads on hypersonic vehicles and their capability for both attached and non-attached turbulent boundary flow.

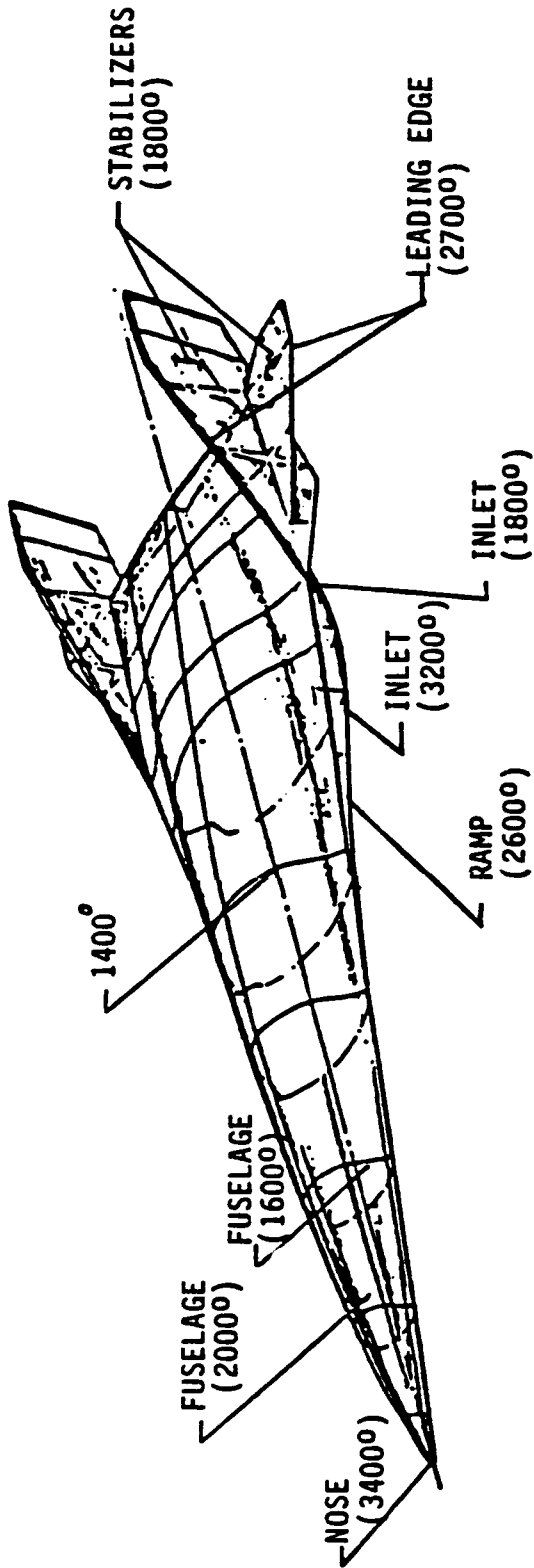
## II. AEROACOUSTIC LOAD PREDICTION

### 1. Attached Flows-Smooth and Rough Surfaces

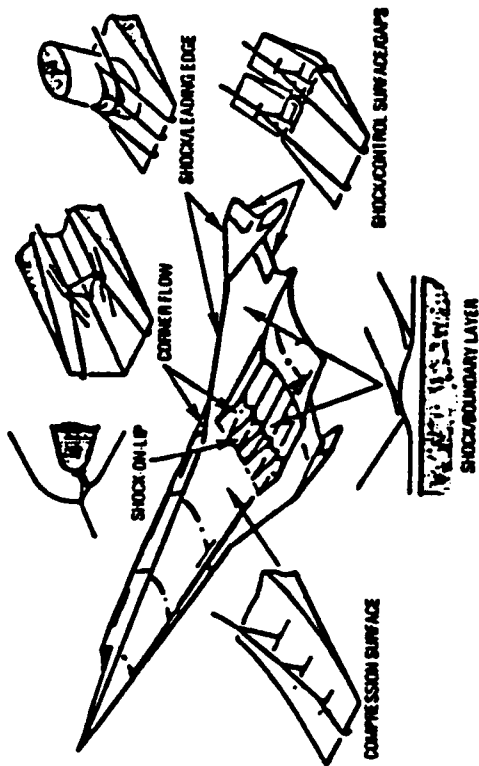
#### a. Smooth Surfaces

The rms pressure fluctuations for the supersonic/hypersonic attached turbulent boundary layer are a function of the boundary dynamic pressure, Mach number, and wall temperature ratio. Experimental data have confirmed this scaling as well as prediction models (References 1, 2 and 3). The prediction models have proceeded from the incompressible flow to include compressibility effects and heat transfer effects.

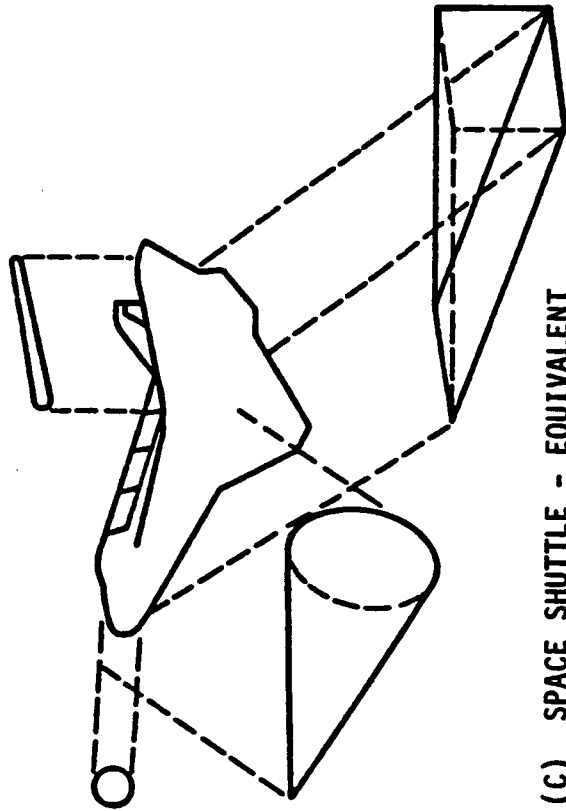
For subsonic conditions Lilley (Reference 4) had found that the normalized rms pressure fluctuations can be found by the expression  $1.7 < \tilde{p}/\tau_w < 3$  for  $M < 1$  and can rise to a value of 5.6 at



(A) BLENDED WING BODY (NASP) TYPICAL SURFACE TEMPERATURE LEVELS (°F)



(B) GENERIC NASP-SHOCK/BOUNDARY LAYER INTERACTION CHARACTERISTICS



(C) SPACE SHUTTLE - EQUIVALENT SHAPES FOR INVISCID/VISCOUS PREDICTIONS

Figure 1. Hypersonic Space Transportation Systems with Flow Interaction Regimes

a Mach number of 10. A more useful expression is in terms of free stream conditions and can be expressed for zero Mach number (incompressible) in the form of

$$\tilde{p}/q_\infty = 0.006$$

This ratio has compared favorably with experimental data (References 5, 6 and 7) and is the starting point for the development of prediction models for the supersonic/hypersonic conditions based on experimental data and fluid dynamic principles. The expressions for the rms pressure fluctuations and power spectra have been derived in Reference (3) to account for viscous effects in addition to compressibility and heat transfer. For a smooth wall and considering the boundary layer displacement and thickness and velocity as characteristic length and velocity respectively these equations are:

$$\tilde{p}/q = 0.006 F_c^{\lambda(1+b)} \quad (1)$$

$$\frac{\phi(\omega)v}{q^2 l} = \frac{2.293 \times 10^{-5} F_c^{-0.5733}}{1 + F_c^{2.867} \left(\frac{l}{V}\omega\right)^2} \quad (2)$$

$$F_c = \frac{C_{f_i}}{C_{f_c}} = h^*/h_e = \frac{1}{2} + \frac{h_w}{h_{aw}} \left(\frac{1}{2} + r \frac{\gamma-1}{4} M_e^2\right) + 0.22r \frac{\gamma-1}{2} M_e^2 \quad (3)$$

with

$$\lambda = [2m - (1+n)]/(3+n) \quad \text{and} \quad b = 2(m+1)/[(1+n) - 2m] \quad (4)$$

where  $n$  and  $m$  are velocity  $[u/u_e = (\gamma/\delta)^{1/n}]$  and viscosity  $[\mu/\mu_e \sim (T/T_e)^m]$  power law exponents respectively.

Using realistic values of velocity power exponent ( $7 \leq n \leq 12$ ) together with viscous power exponent ( $0.6 < m < 1.0$ , values of 'b' fall in the range of  $0.3 < b < 0.6$  which are consistent with values experimentally determined in References (1 and 2) in the range of  $0.3 < b < 0.5$ .

For the values of  $m = 0.7$  and  $n = 9$  the value of  $b$  is equal to 0.4 and Equation 1 reduces to  $p/q = 0.006/F_c$ . Thus in the case of incompressible flow  $F_c \rightarrow$  unity and reduces to the Lowson (Reference 5) result as given above. The value of the constant 0.006, while accepted by the scientific community, is believed to be in error as a result of instrumentation gage size limitations (Reference 8). The error could yield incompressible values of 0.010 in its place. Until further definitions can be made concerning transducer size error, the following will continue the use of the value 0.006.

A comparison of the predicted normalized rms pressure and data with compressibility and heat transfer is shown in Figure (2). This figure shows the expected drop rms pressure with increasing Mach number. The results of Lowson is shown for the adiabatic wall.

#### POWER SPECTRA

Equation (2) is the power spectra; this equation has been developed from the power spectrum density developed by Houbolt (Reference 9). This development is based on experimental data which indicates that the spectrum peaks near the wall within the boundary layer and decays away from the wall. Thus the power spectral density is considered as a function of the spectrum of the form:

$$\phi(\omega) = \frac{\phi(0)}{1+K^2\omega^2} \quad (5)$$

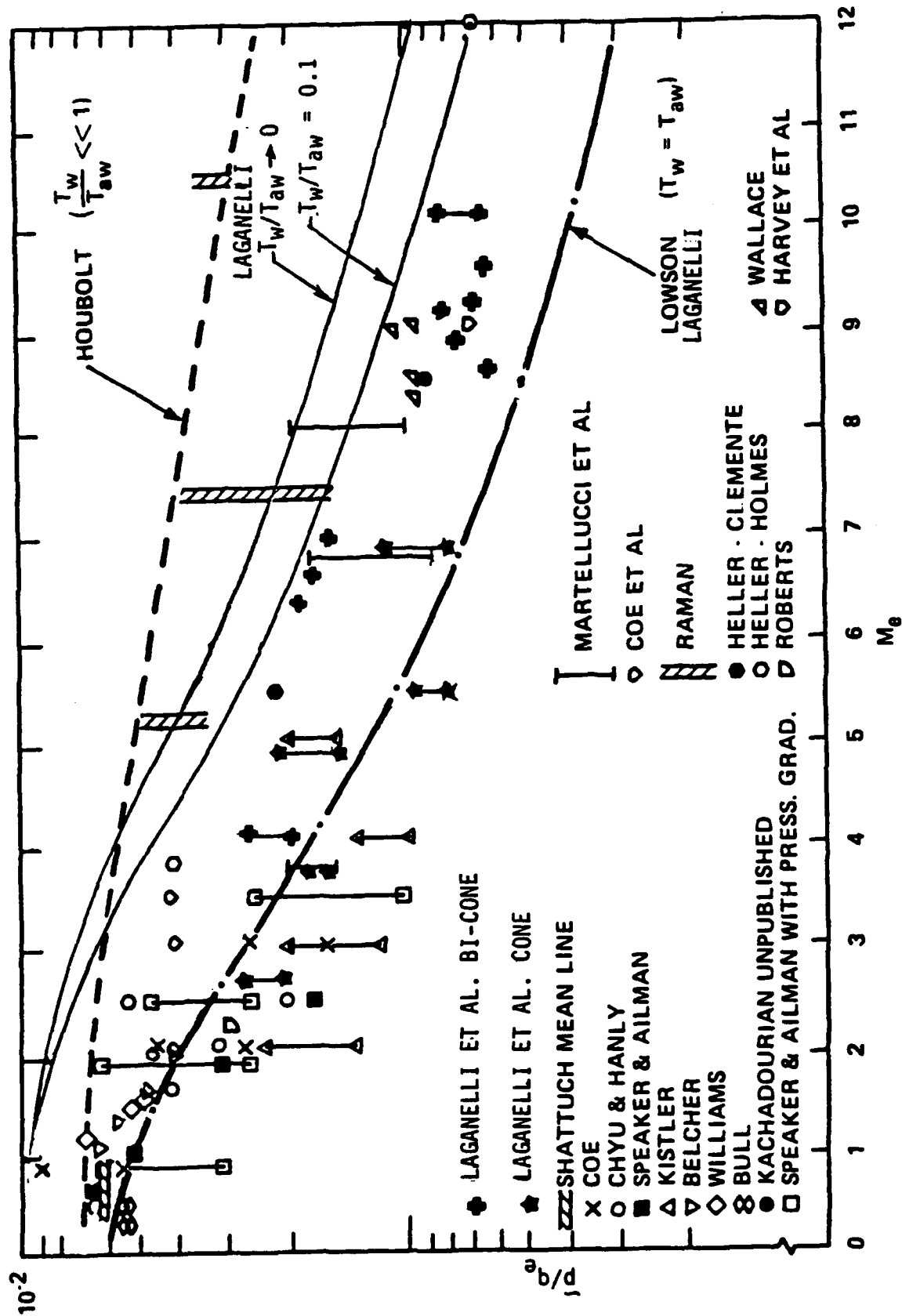


Figure 2. RMS Pressure Variation with Mach Number - Attached Turbulent Boundary Layer Flow (Smooth Wall) - References 1 and 2



where the parameter  $K$  is dependent on the local properties of the flow; these are the characteristic length  $l$  and the characteristic velocity  $v$ . The product in the denominator is a Strouhal number. Thus the spectra scale on this number. For this form of the spectrum equation the associated correlation function is an exponential function and leads to a scale of the turbulence of the order of the characteristic length.

By definition the rms pressure is related to the power spectra by:

$$(\bar{p}/q)^2 = \frac{\phi(0)\pi/2}{k'(\bar{l}/v)q^2} \quad (6)$$

Equation (2) is obtained with this relation and the rms pressure fluctuation Equation (1). The details of this derivation is given in References (1,2 and 3). The derivation involves the application of fluid dynamic principles as well as experimental data to include the effects of compressibility and heat transfer. This is in contrast with the earlier work of Reference (10) which uses an empirical relation from curve-fit of the experimental data. The power spectra experimental data is compared with the predictions of Equation (2) in Figure (3) (Reference 1). Both incompressible and compressible data are shown in this figure. There is good agreement of the prediction value with experimental data.

#### CROSS-POWER SPECTRA

The co-power spectral density or the narrow band space correlation function is needed to describe the spatial correlation properties of the fluctuating pressures field on a structure surface for the purpose of calculating the induced mean-square response of the structure. The empirical relations from

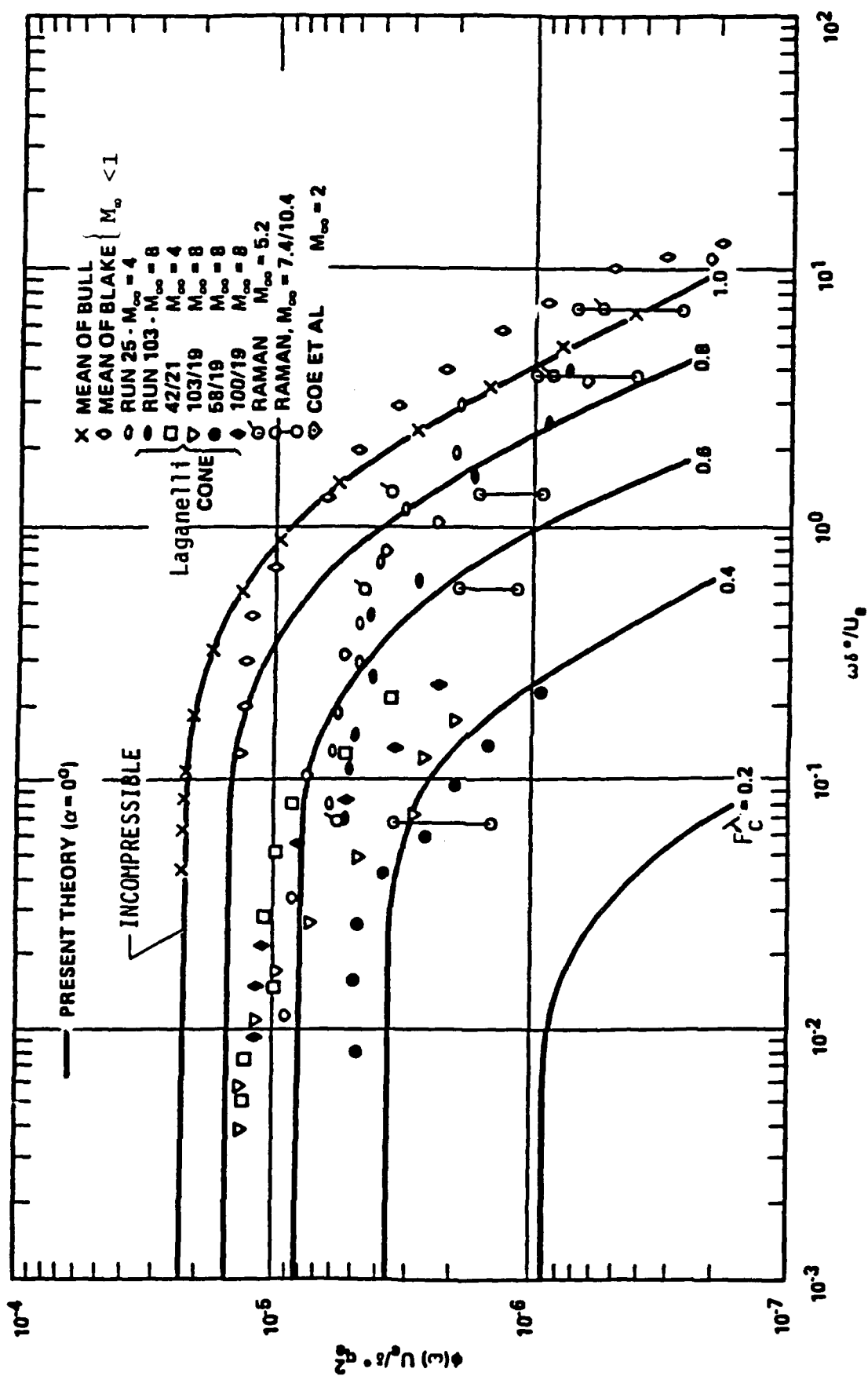


Figure 3. Comparison of Normalized Spectral Measurements (Reference 1) and Theory

experimental data have been derived in References (5,10, and 11).

#### b. Rough Surface

The acoustic loads can be augmented in the presence of rough surfaces. Equation (1) has been extended in Reference (12) to include the increase in wall skin friction due to the roughness elements. Good agreement with experimental measurements have been obtained (References 3 and 12).

### 2. Separated Flows

Separated flows over a vehicle in flight due to localized pressure gradients caused primarily by the body shape leads to enhanced fluctuating pressure load on the body surface. A number of these typical separations have been discussed in References (10,11). These have been categorized as 2D separation flows having mean separation and re-attachment lines normal to the free stream. Large fluctuating pressure levels are produced at the reattachment point with lower pressures between the separation point and reattachment point. An example is the blunt body induced separation which can occur at cone-cylinder and flare-cylinder expansion corners at subsonic Mach numbers. Expansion induced separated flows occur downstream of expansion corners such as regions aft of cone-cylinder junctions, rearward-facing steps and the near wake of a boattail. Empirical relations based primarily on curve-fitting the experimental data for the rms pressure have been obtained by Robertson (References 10,11). These have been used for the prediction of the aeroacoustic loads. The inclusion of fluid dynamic principles in deriving these empirical relations would have put them on a more firmer base and enhanced their application to extended conditions. The methodology as presented by Laganelli and Wolfe (Reference 3) does this and is discussed below.

### 3. Shock/Boundary Layer Interaction (non-attached)

#### a. 2D Compression Corner

Experimental data on shock wave boundary layer interaction have been obtained for several two dimensional and three dimensional configurations. The simplest geometry is the 2D compression corner followed by a 3D swept-fin configuration. The 2D flow is typical of that of a flare-induced or step induced separation.

Rms pressure fluctuations and associated power spectra for this 2D flow have been obtained in a series of experiments and given in References (13, 14, 15, and 16) for the shock/boundary layer characteristics of flow over a 24 degree compression ramp. The data is limited to the Mach range  $\leq 3$ .

A typical configuration is shown on Figure (4a) (Reference 14) showing the boundary layer edge and the coalescence of the wave system into a single shock for a free stream Mach number of 2.85. Note that Mach number one line within the boundary layer structure and the distance along the surface is measured from the corner. the mean pressure distribution at the wall is shown in Figure (4b); the mean pressure shown is relative to the approach flow and starts to rise (to a peak of about 4) upstream of the corner creating a subsonic flow separation region that reattaches on the ramp. The extent of this region and the strength of the shock is dependent upon the angle of deflection of the ramp.

The rms pressure fluctuation is shown on Figure (4c) and is the result of the conversion of the mean flow energy into random fluctuations by the shock wave system. The normalized rms fluctuating pressure is characterized by peaks relative to the points of separation and reattachment. The peak value, located at

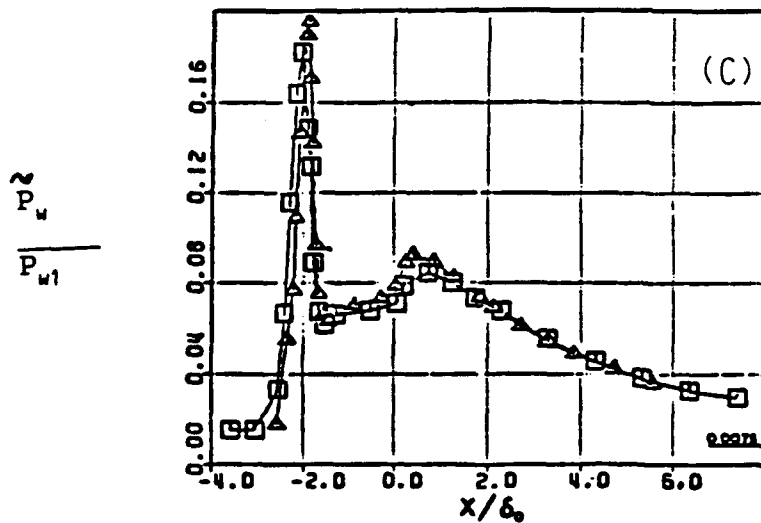
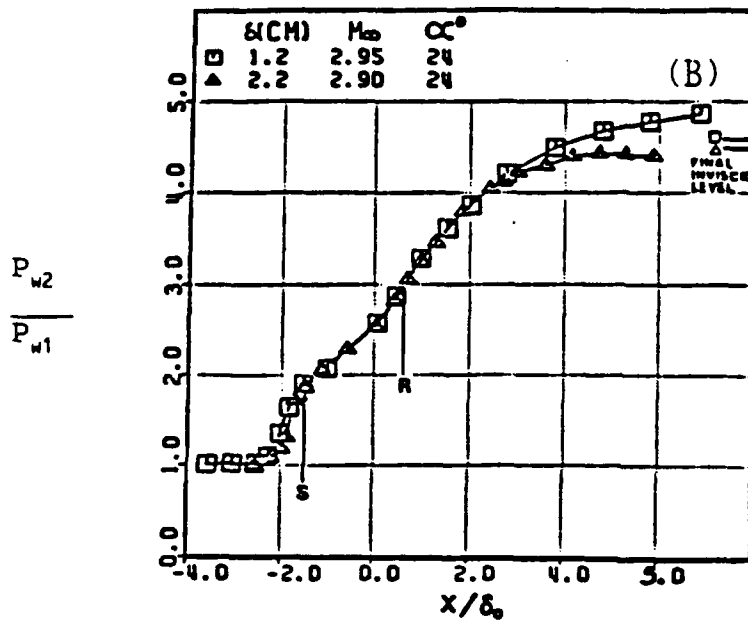
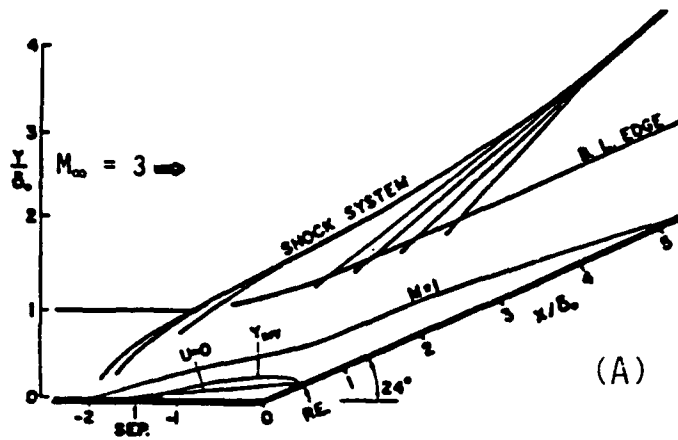


Figure 4. Typical Example of Compression Corner Shock/Boundary Layer Interaction (24° Ramp) - Reference 14

approximately two times the approach flow boundary layer thickness upstream of the corner, is characteristic of shock oscillations observed in other experiments experiencing 2D flow separation.

Dolling and Or (Reference 13) have obtained results for the rms fluctuation pressure for several ramp angles. These pressures normalized by the upstream static wall pressure are shown in Figure (5). As expected, this figure shows that the rms peak pressure fluctuation as well as the plateau levels experienced a decrease with decreasing shock strength. However, even at the lowest ramp angle (attached flow) there is a significant rise in the rms fluctuating peak level.

b. 3D Swept-Fin

Additional results for the 2D compression corner interactions as part of the investigations in swept shock wave/turbulent boundary layer interactions were obtained by Tran (Reference 17). This study focused on the unsteadiness in these interactions. It was shown that the 2D compression corner was inherently different in their response to the same approach flow.

The results are shown in Figure (6) for various sharp fin generated interactions for both mean and rms pressure fluctuation. The mean pressure distribution in part A of the figure shows locations for the upstream influence (UI) and coalescence (C) line where the latter is the location of the flow separation. The UI line corresponds to the position of initial pressure rise while the coalescence line does not appear to relate with any flow feature of the mean distribution. Both mean pressure (20 degree fin data shown) and rms pressure show a dependence on shock strength as was experienced in the 2D ramp experiments. However, the rms peak for the 3D swept interaction is approximately one-half of the value experienced in the 2D ramp rise for similar approach flow and

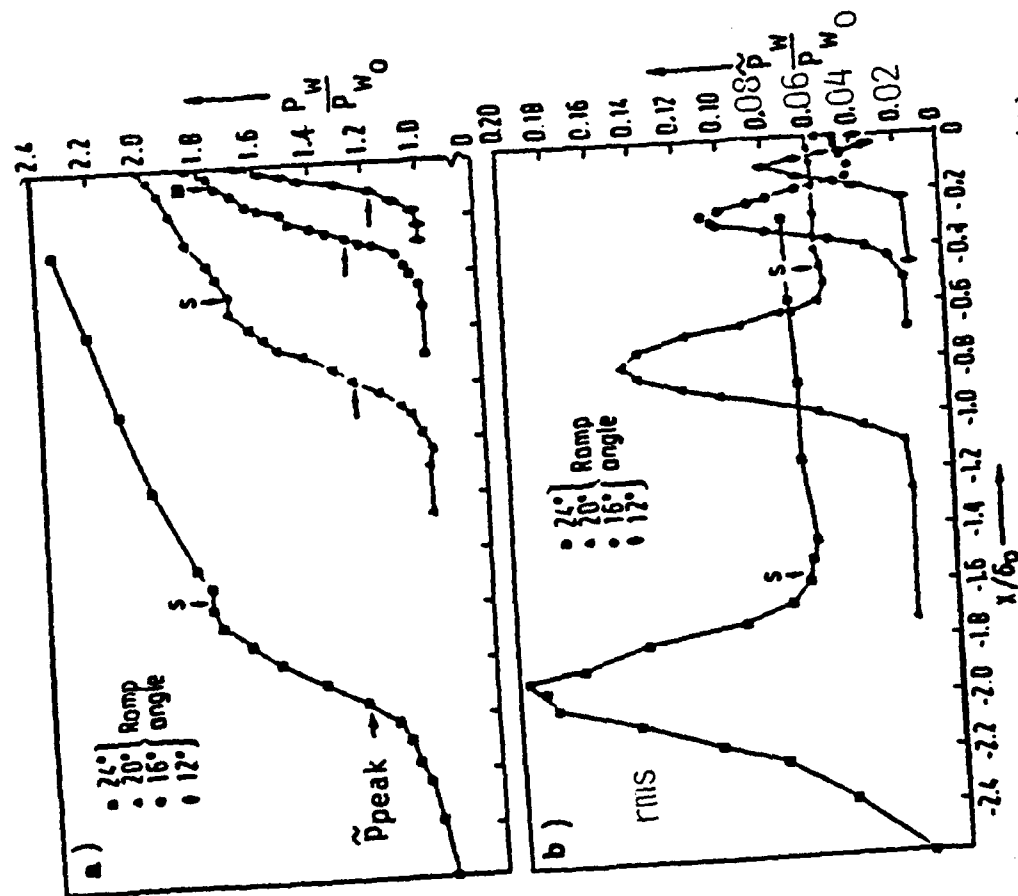


Figure 5. RMS Pressure Distribution with Shock Strength (2D Interaction) Reference 13

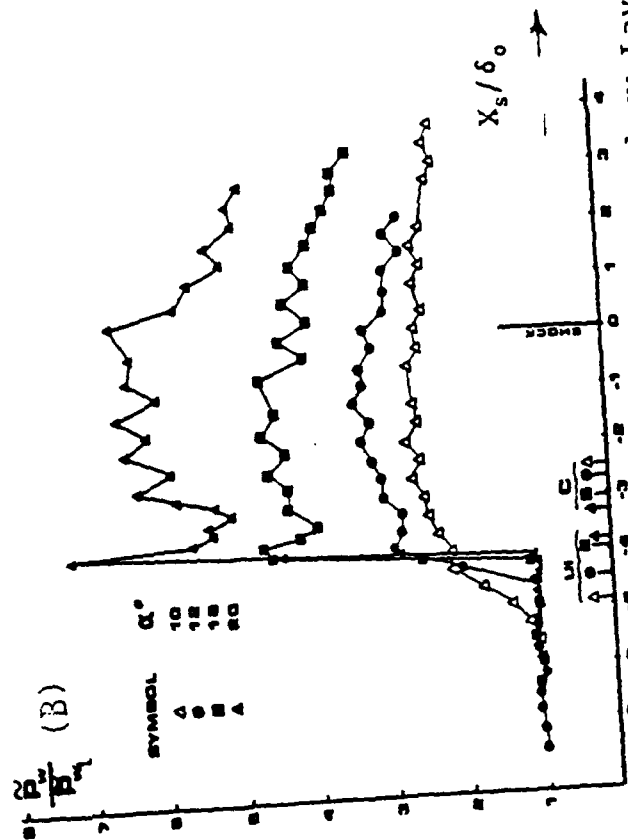


Figure 6. Fin Generated (3D) Shock/Boundary Layer Interactions for Mean (A) and Fluctuating (B) Pressure - References 19 and 20

similar shock strength. As shown in the figure, the rms fluctuation pressure peaks suggests an intermittent action at the start of the interaction even though the mean pressure has not shown a significant increase.

Tran (References 17, 18) has made a comparison of 2D ramp and swept type interactions. The comparison includes overall inviscid pressure rise, the peak rms pressure fluctuations, pressure gradient distribution, and the spatial extent of large amplitude disturbance. Figure (7) shows a comparison of the rms pressure fluctuations for the 2D ramp and swept interactions. The rms peak increases with shock strength and magnitude and for a given inviscid pressure rise the swept interaction is approximately half of that of the corresponding 2D ramp interaction.

#### c. Correlation of rms Pressure and Power Spectra

The data for the interacting shock wave/boundary flows discussed in the last section have been used to obtain acoustic load algorithms useful in applications. As shown above the normalized rms fluctuating pressure distributions for 2D ramp (corner flow) and 3D swept shock interactions show a peak occurrence and plateau region prior to its reduction to the approach flow levels. Thus the algorithms must focus on these regions. Any prediction results must also incorporate the approach flow characteristics. Correlations for peak rms pressure and plateau level rms pressure have been made by Laganelli and Wolfe (Reference 3). These correlations have not required the a priori knowledge of the initial pressure gradient and spatial extent through the interaction region for its application.

The plateau level of the rms pressure fluctuation is assumed to correlate with the approach flow and shock strength of the form:



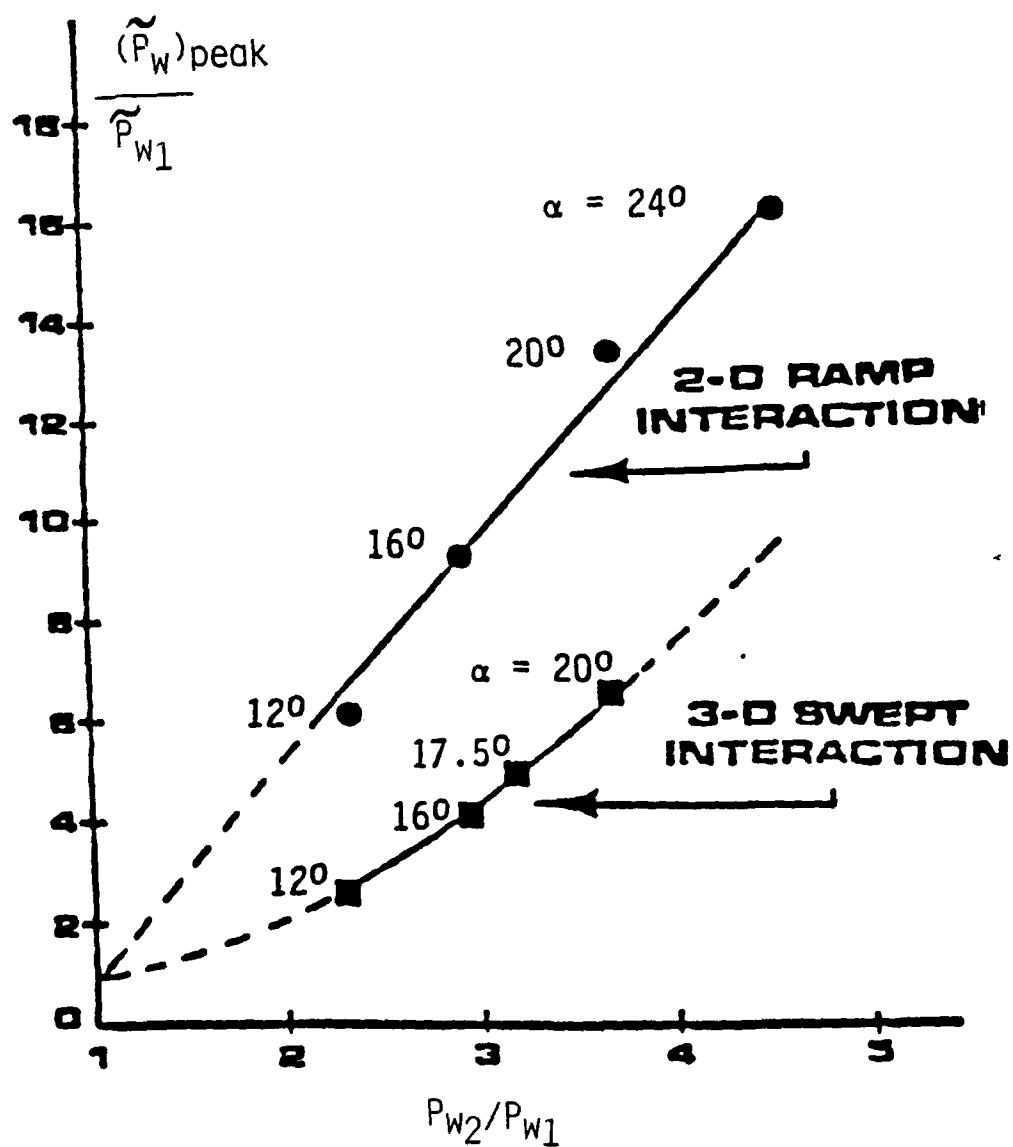


Figure 7. Peak rms Pressure Variation for 2D/3D Interaction with Shock Strength-Reference 17

$$\left(\frac{\bar{P}_{W2}}{P_{W2}}\right)_{\text{plat}} = \left(\frac{\bar{P}_{W1}}{P_{W1}}\right) \left(\frac{P_{W2}}{P_{W1}}\right)_{\text{max}} \quad (7)$$

Using Equation (1) the rms pressure for the approach flow can be written as

$$\frac{(\bar{P}_{W1})}{P_{W1}} = 0.006 \frac{\gamma}{2} M_1^2 F_c^{\lambda(1+b)} \quad (8)$$

with  $q_1$  the dynamic pressure

The maximum inviscid pressure rise (shock strength) is given by the oblique shock relation. This is

$$\left(\frac{P_{W2}}{P_{W1}}\right)_{\text{max}} = \frac{2\gamma M_1^2 \sin^2 \theta_s - (\gamma - 1)}{\gamma + 1} \quad (9)$$

In this equation, the shock angle has been approximated (Reference 2) and is given by the relation

$$\theta_s = \alpha + \sin^{-1} (1/M_1) \quad (10)$$

for  $\alpha$  the shock generator angle.

For the 2D corner flow at a ramp angle of  $24^\circ$ , the maximum inviscid pressure rise becomes  $(P_{we}/P_{wi})_{\text{max}} = 4.6$  and the normalized rms pressure fluctuation, Equation (7) has a value of 0.078 which shows good agreement with the results of Figure (5). On a 16 degree ramp the normalized fluctuating pressure in the plateau region has a value of 0.0552 which also shows good comparison with Figure (5).

### 3D SHOCK WAVE/BOUNDARY INTERACTIONS

For 3D flow, the shock generator angle has to be modified (Reference 3) to account for interactions which occurred closer to the shock generator. Observations of maximum heating (shear) locations indicate this and suggests that the maximum rms pressure fluctuations will also occur at this location. The location of peak mean pressure and heating occurs approximately along a streamline from the shock generator leading edge. The angle  $\phi$  between this ray and the freestream direction has been correlated as  $\phi = 0.24 (\theta_s - \alpha) + \alpha$ . The modified shock angle has been generalized to include a constant,  $\beta$ , and is given in the form

$$\phi = \alpha + \beta \sin^{-1} (1/M) \quad (11)$$

where

- (i)  $\beta = \text{unity}$  @ 2D flow interaction ( $\phi = \theta_s$ )
- (ii)  $\frac{1}{2} < \beta < 1$  @ rms peak fluctuation pressures for swept shock/boundary layer 3D interactions.

Since the maximum rms fluctuating pressure can be expected to occur at the approximate locations of peak pressure and heating (shear), the normalized rms fluctuating pressure can be expressed in terms of the shock strength with the new definition of shock angle and  $\beta$  determined from experimental measurements. Thus the normalized peak rms fluctuating pressure for a 2D/3D shock boundary layer interactions is correlated as

$$\frac{(\bar{P}_W)_{\text{peak}}}{\bar{P}_{W1}} = -1.181 + 1.713 (P_{W2}/P_{W1}) + 0.468 (P_{W2}/P_{W1})^2 \quad (12)$$

for  $P_{W2}/P_{W1} > 1$ . The inviscid pressure rise is obtained using Equation (8) with the new angle  $\phi$  for  $\beta = 0.6$ .

The correlation is shown in Figure (8) compared with experimental data of Figure (7) as well as Reference (21). In the plateau region of a swept 3D-shock/boundary layer interaction Equation (7) can be used with  $\beta = 0.6$  in Equation (11). For example, for the fin generated swept shock experiments represented in Figure (6) the normalized rms plateau pressure has a value of 0.0452 for a fin angle of  $\alpha = 20$  degrees and this value is representative of the levels shown in the figure. Similar results are easily obtained for other fin angles and these also show good comparison with measured data.

#### POWER SPECTRA

An increase in the power spectra of the pressure fluctuation due to the interaction phenomena is experienced above the attached flow level. While the spectra tend to converge toward a common level and slope at high frequencies, a significant variation exists between the separated flow spectra and that of the attached flow distribution. This can be seen from Figure (9) for a 24 degree ramp. It is evident from the figure that the low frequency components of the fluctuating pressures are increased in intensity while the intermediate and high frequency retain the characteristics of the approach boundary layer (which is attached). The approach flow displays a characteristics that is typical of power spectra that includes low frequency peaks associated with facility generated noise. An excellent comparison with the prediction of Equation (2) is shown in part A of the figure. The part B of this figure displays broad-band characteristics of the spectra at several locations relative to the corner of the ramp.

For the correlation of data, the approach flow boundary layer parameters are generally selected for normalizing the power spectra for the convenience of engineering applications since local boundary layer characteristics in the interaction region are not

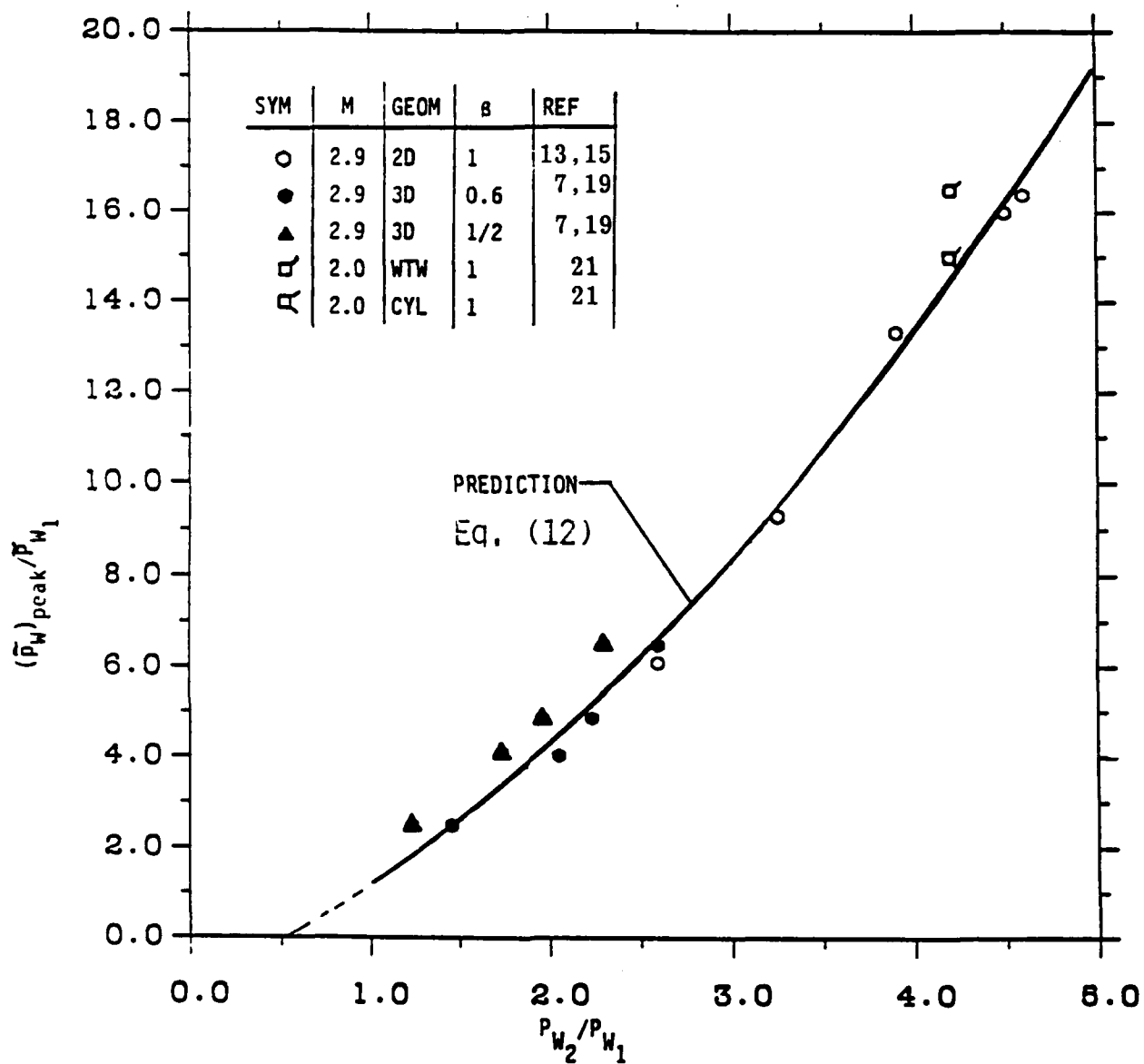


Figure 8. Correlation of Peak rms Pressure for Shock/Boundary Layer Interactions

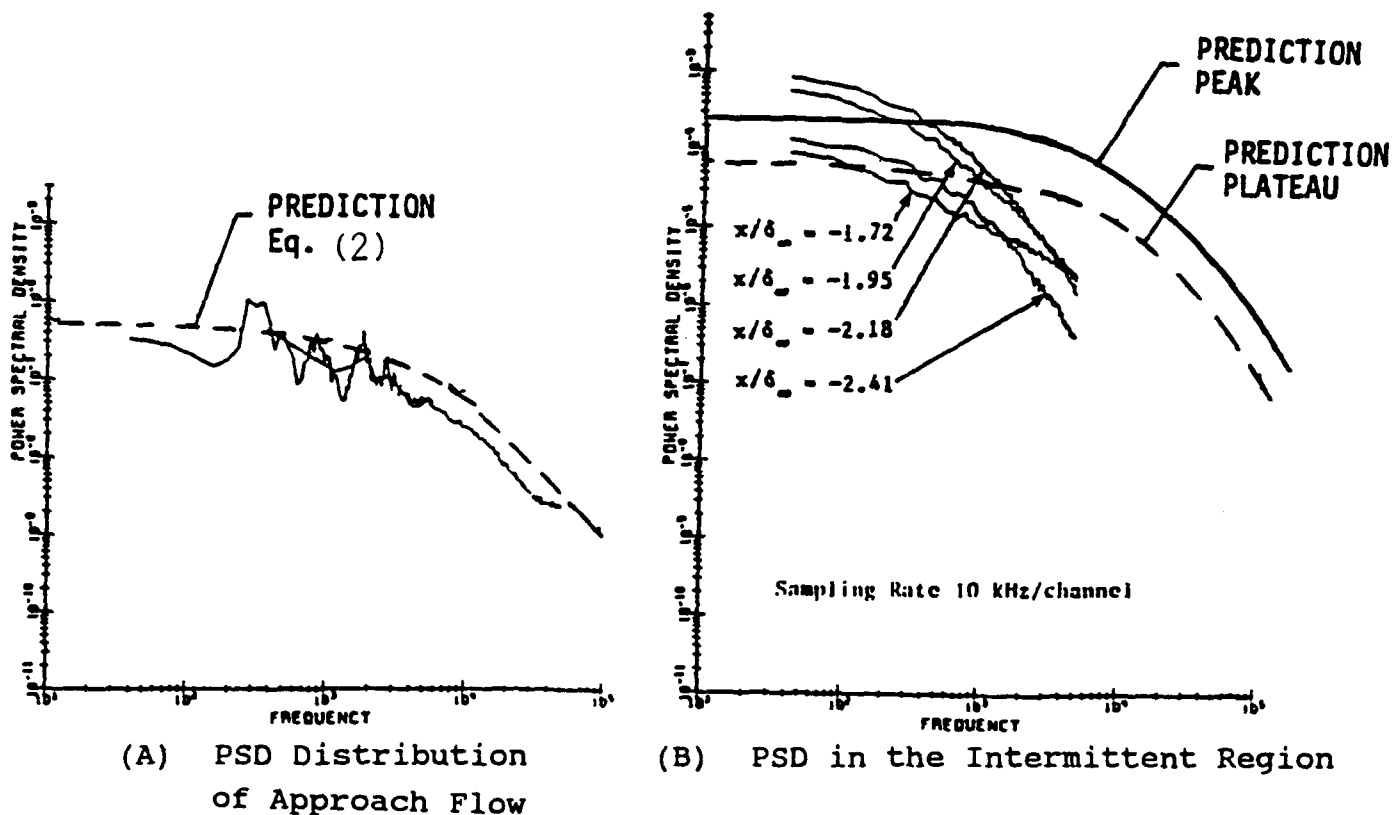


Figure 9. Comparison of Prediction Technique to Measured Power Spectral Density Data for a 24° Compression Ramp

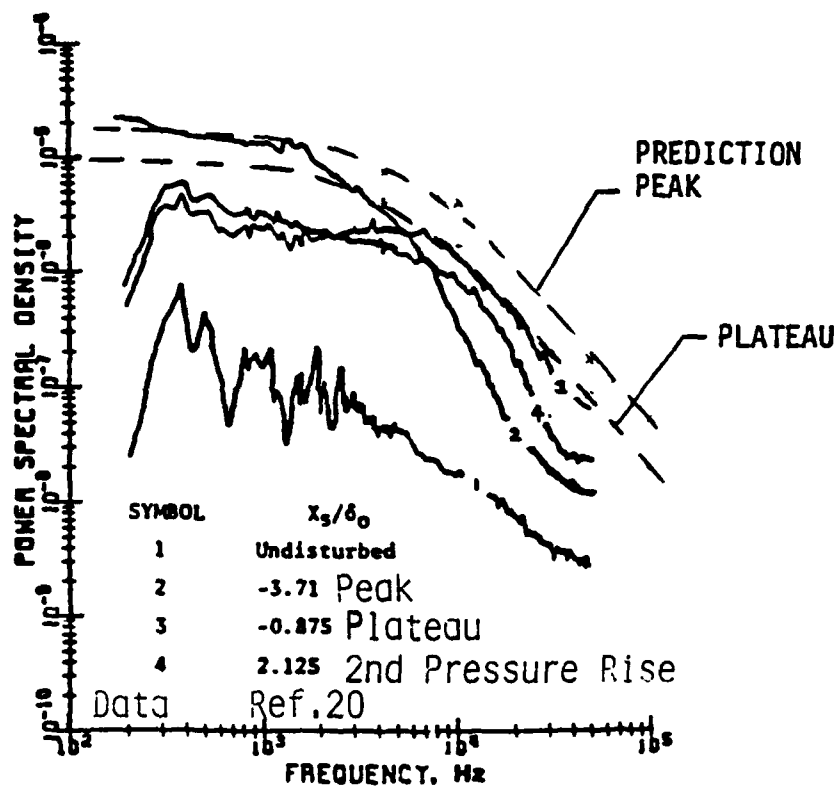


Figure 10. Comparison of Prediction Technique to Measured Power Spectral Density Data for a 20° Fin Shock Generator

well defined and sometimes not easily accessible. The correlation (Reference 3) of the power spectra requires the amplitude of the power spectra at low frequencies of the form

$$\phi(f \rightarrow 0) \rightarrow \frac{4 q^2 \ell}{v} F_c^{1.433} (\tilde{p}/q)^2 \quad (13)$$

With normalized rms pressure put in terms of the approach flow and peak and/or plateau levels, the amplitude of the power spectra in the plateau pressure region with the value from low frequency is then given by

$$\phi(f \rightarrow 0)_{\text{plateau}} \rightarrow \phi(f \rightarrow 0)_{\text{flow approach}} \left[ \frac{M_1^2 (\gamma+1) (P_{W2}/P_{W1})_{\text{max}}^2 \sin^2 (\theta_5 - \alpha)}{(\gamma-1) M_1^2 \sin^2 \theta_5 + 2} \right]^2 \quad (14)$$

Similarly, if the dynamic pressure is evaluated at plateau levels, the amplitude of the peak power spectra is given by

$$\phi(f \rightarrow 0)_{\text{peak}} \rightarrow \phi(f \rightarrow 0)_{\text{flow approach}} \left[ \frac{(\tilde{p})_{\text{peak}}}{\tilde{p}_{W1}} \left( \frac{M_1}{M_2} \right)^2 \frac{P_{W1}}{P_p} \right]^2 \quad (15)$$

where the Mach numbers are related by the oblique shock relations.

Figure (9b) shows the peak and plateau level power spectral density predictions compared to the corner data of Reference (19). It is seen that the predicted amplitudes are reasonable but the spectral distribution is over predicted in the high frequency range although the rate of drop of the curves are reasonably close.

Figure (10) compares the prediction results to the swept shock wave/boundary layer interaction of Reference (20). It appears that

the roll-off characteristics for the 3D type interactions are more commensurate with attached flow behavior thereby allowing for a reasonable engineering estimate of the power spectra.

#### 4. Application to McDonnell-Douglas Blended Wing Body

The prediction techniques discussed in the previous sections have been applied to the McDonnell-Douglas Blended Wing Body (BWB) by Laganelli (Reference 22).

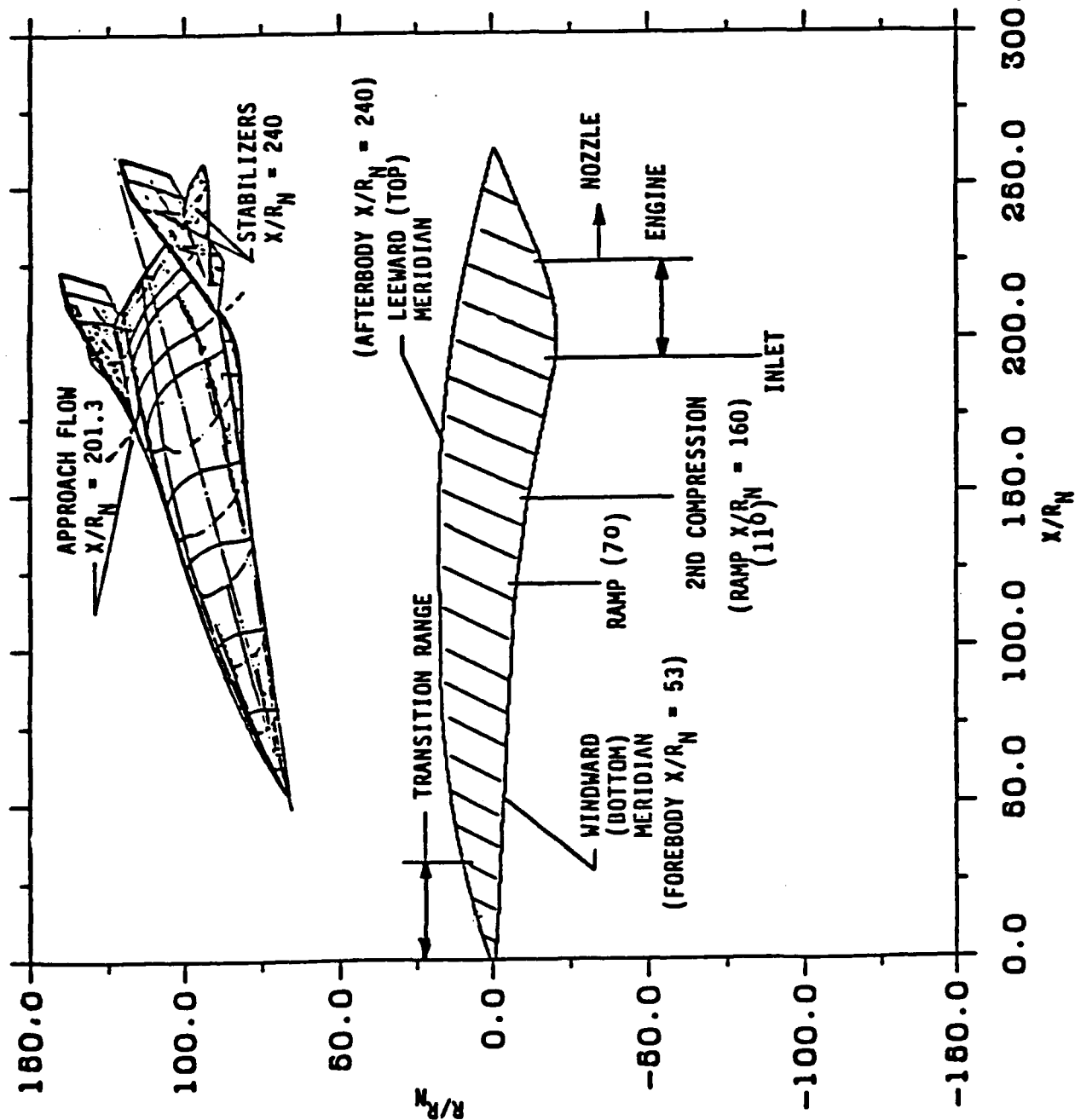
##### a. BWB Flowfield

The BWB configuration is shown in Figure (11). Note that the body includes vertical and horizontal stabilizers which will have shock boundary layer interactions in addition to the typical attached boundary over the frontal part of the body. Thus the spatial and temporal resolution of the power spectra will depend upon the location along the body and the mission profile. For this analysis several vehicle stations were selected for investigation for the ascent phase of high dynamic pressure and heating flux and for the descent phase of lower dynamic pressure and heating rates. The parameters for the boundary layer flow over the body were obtained utilizing a PNS (parabolized Navier-Stokes) computer program. These parameters included the shock/boundary layer interactions from the vertical/horizontal stabilizers.

Figure (11) also shows the body region of interest and the flight conditions which is being investigated. Trajectory (Mach number and altitude), transition and wall temperature are identified for nominal freestream dynamic pressure conditions of 1000 and 2600 psf respectively.

The SAIC PNS codes (References 23, 24), SCRAM and SCRINT were used to generated a 3D parabolized Navier-Stokes turbulent flow





# **CONDITIONS \***

$R_N = 4.5$  INCHES

$Q_\infty = 1000$  PSF

ALT XTR  $T_w$

| $H_\infty$ | (KFT) | (FT) | ( $^\circ R$ ) | SURFACE |
|------------|-------|------|----------------|---------|
|------------|-------|------|----------------|---------|

|    |       |    |      |     |
|----|-------|----|------|-----|
| 4  | 71    | 6  | 540  | B/T |
| 6  | 88.4  | 6  | 1600 | B/T |
| 10 | 110.9 | 12 | 2000 | B/T |
| 15 | 129.9 | 15 | 1600 | B/T |
| 20 | 144.1 | 0  | 1600 | B/T |
| 25 | 155.7 | 0  | 1600 | B/T |

$Q_\infty = 2600$  PSF

|    |       |   |      |     |
|----|-------|---|------|-----|
| 6  | 68.0  | 0 | 1600 | B   |
| 10 | 89.75 | 0 | 1600 | B/T |
| 15 | 107.6 | 0 | 1600 | B   |
| 20 | 120.5 | 0 | 1600 | B   |
| 25 | 131.5 | 0 | 1600 | B   |

B - Bottom (Windward)  
T - Top (Leeward)

\*TRANSITION ZONES HAVE BEEN DESIGNATED FOR THE  $Q_\infty = 1000$  psf TRAJECTORY WHILE ALL TURBULENT CONDITIONS DESIGNATED FOR  $Q_\infty = 2600$  psf TRAJECTORY

Figure 11. Blended Wing Body Investigation Regions Model

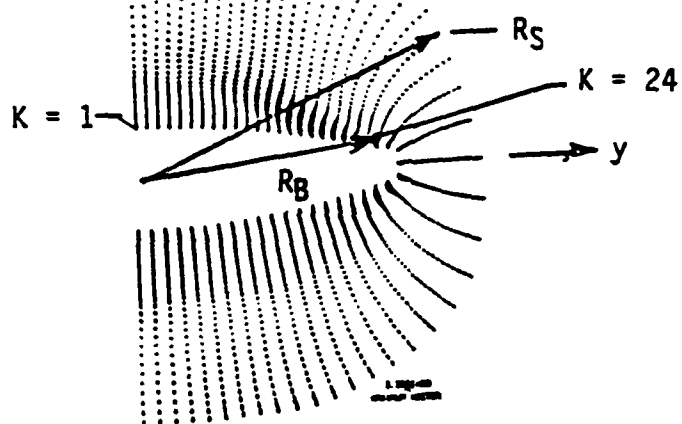
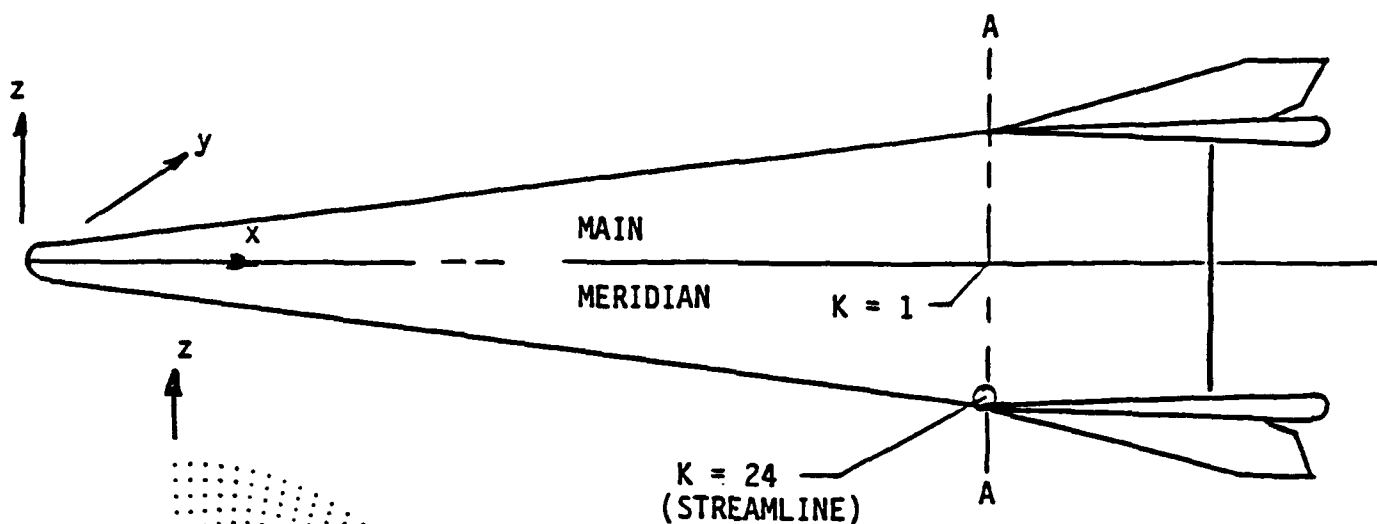
over the 3% BWB (3 feet) without horizontal/vertical stabilizers. These codes use a space marching finite-difference technique to solve the Navier-Stokes equations for supersonic/hypersonic viscous flows for either 3D or 2D planar/axisymmetric flows. The solutions were generated on the main meridian of the windward (bottom) and leeward (top) surfaces of the BWB.

The flowfield generated determined the general characteristics of the approach flow in the region of the stabilizer intersection. Figure (12) shows the SAIC 3D PNS results at the 77% axial station (stabilizer intersection) for the 3% BWB configuration for a freestream Mach number of 12.4. The table shown compares the difference of using 2D PNS solutions (main meridian at  $K = 1$ ) to establish approach flow conditions leading to the horizontal stabilizer (HS) and vertical stabilizer (VS) shock/boundary layer interactions region ( $K = 24$  streamline in the 3D PNS solution).

Figure (12) shows the strong cross-flow effects as denoted by the shock curvature (Section A-A). However, since the similarity parameters of Mach and unit Reynolds number do not vary significantly and the ratio of the boundary layer thickness to the flowfield thickness is maintained the use of 2D PNS (main meridian) appear to be adequate for engineering level estimates of the approach flow leading to the HS/VS shock/boundary layer interactions region.

#### b. BWB Acoustic Loads-Attached Turbulent Boundary Flow

A number of solutions of acoustic loads were studied in Reference (22). These included the rms pressure fluctuations, power spectra, and sound pressure level as well as mean pressure and heat transfer along the top and bottom meridian of the BWB for attached turbulent boundary layer flow conditions. The trajectory



#### CONDITIONS

$$H_T/H_\infty = 0.99$$

$$Re_\infty/ft = 5.8 \times 10^5$$

$$M_\infty = 12.4$$

$$T_\infty = 164^\circ R$$

$$T_w = 530^\circ R$$

$$\rho_\infty = 1.036 \times 10^{-5} \text{ sl/ft}^3$$

$$P_\infty = 2.9 \text{ psf}$$

A-A 77% LOCATION ( $X/R_N = 201$ )

| K  | P/P <sub>∞</sub> | ρ/ρ <sub>∞</sub> | $u$<br>$\frac{\text{sl}}{\text{ft}^2 \cdot \text{sec}} \times 10^{-7}$ | T/T <sub>∞</sub> | Re/ft<br>$\times 10^5$ | Me <sub>x</sub> | u <sub>e</sub> /u <sub>∞</sub> | δ<br>ft | δ*<br>ft | R <sub>S</sub><br>ft | R <sub>B</sub><br>ft | ΔR <sub>S</sub> /B<br>ft | δ/ΔR <sub>S</sub> /B |
|----|------------------|------------------|--|------------------|------------------------|-----------------|--------------------------------|---------|----------|----------------------|----------------------|--------------------------|----------------------|
| 1  | .46              | .52              | 2.38   | 1.34             | 1.75                   | 9.0             | .98                            | .141    | .107     | .486                 | .131                 | .355                     | 0.14                 |
| 24 | .94              | 1.11             | 3.24   | 2.64             | 2.67                   | 7.4             | .97                            | .013    | .009     | .475                 | .386                 | .089                     | 0.15                 |

Figure 12. Boundary Layer Properties Generated for 3% BWB Using 3D Parabolized Navier-Stokes Solution

and surface locations corresponding to these solutions are given in Figure (11).

The rms fluctuation pressure on the BWB configuration at the Mach number of 10 is shown on Figure (13). These curves show the difference of the rms pressure for two value of free stream dynamic pressure. These two values are the nominal (1000 psf) and the maximum (2600 psf). The differences disappear if the boundary layer edge dynamic pressure is used in the normalization of the rms pressure.

Figure (13) shows the impact of surface geometry on the forebody and ramp on the rms pressure. In general, the rms pressure fluctuation decreased with distance along the top surface while increasing in regions where the static pressure is increased due to ramps.

The power spectra is shown in Figures (14, 15). From these figures it is seen that the normalized power spectral density do not vary significantly along the configuration or from the top to the bottom surfaces. The dimensional forms presented in part (b) of these figures shows the variation in power intensity (energy) represented by the area under the power spectra curve.

Other effects such as the variation of Mach number and wall temperatures on these quantities are shown in Reference (22).

#### c. BWB Acoustic Loads-Shock/Boundary Layer Interaction Regions

The regions on the BWB consisting of the top aftbody ( $x/R_n = 240$  see Figure (11)), horizontal stabilizer (HS) and vertical stabilizer (VS), and the inlet/cowl region will lead to shock/boundary layer interactions. The HS is also subject to

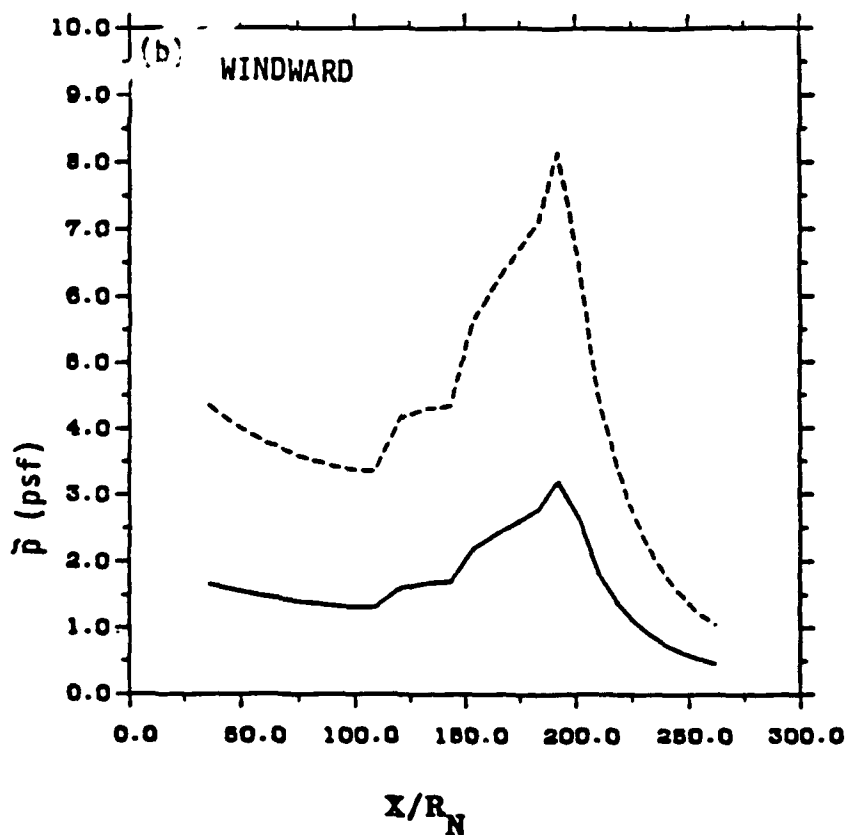
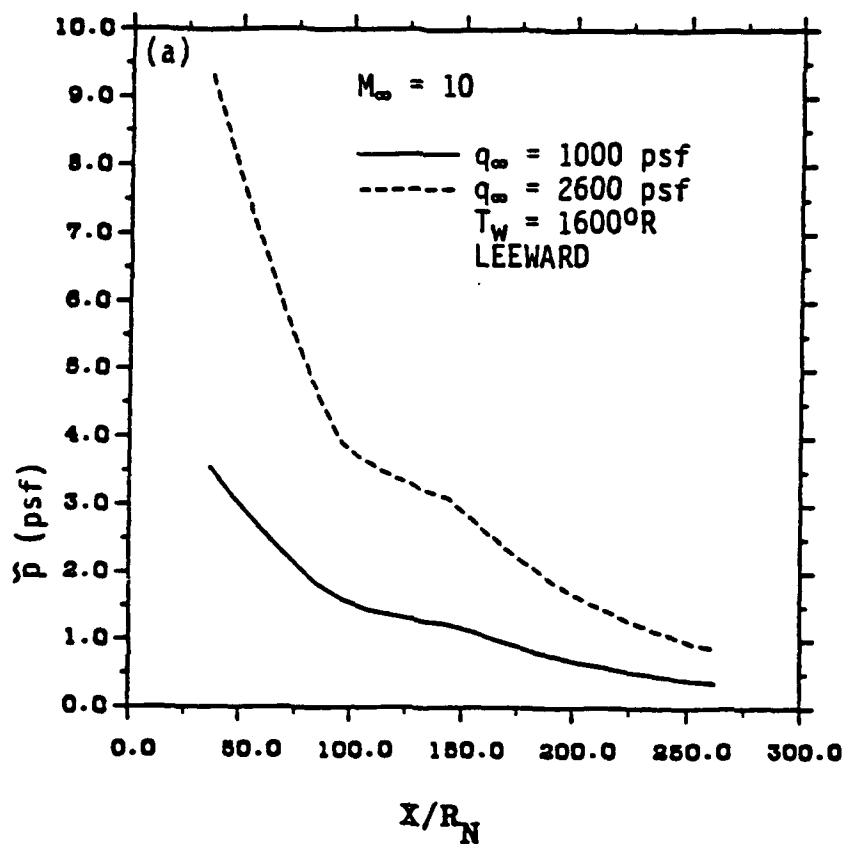


Figure 13. RMS Pressure Distribution on Leeward and Windward Meridians of BWB Configuration at Mach 10

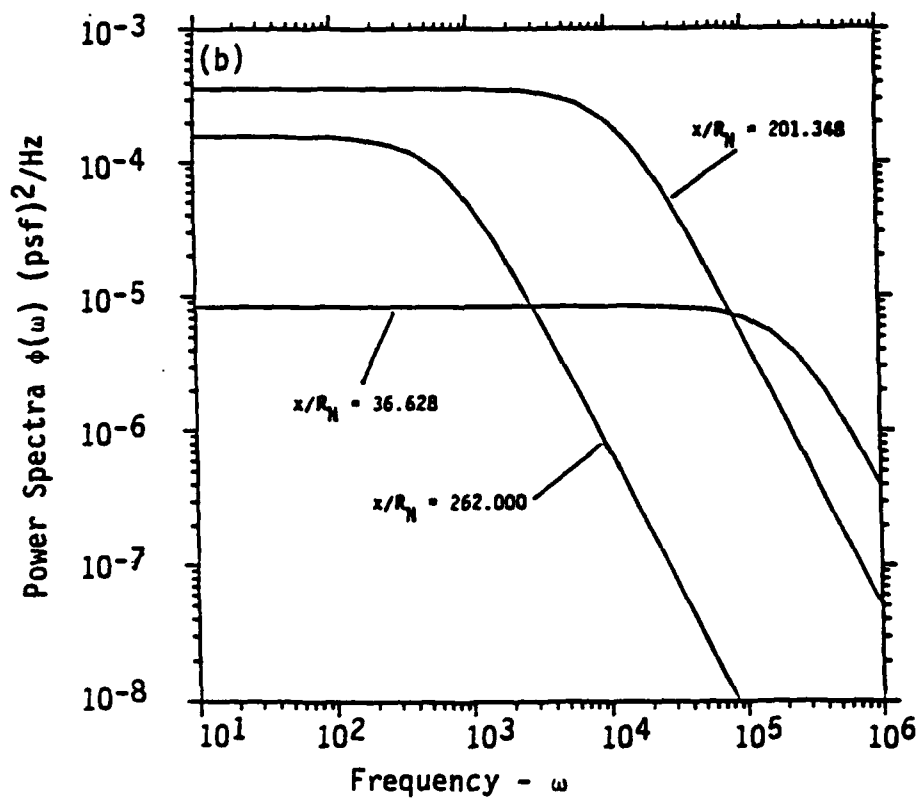
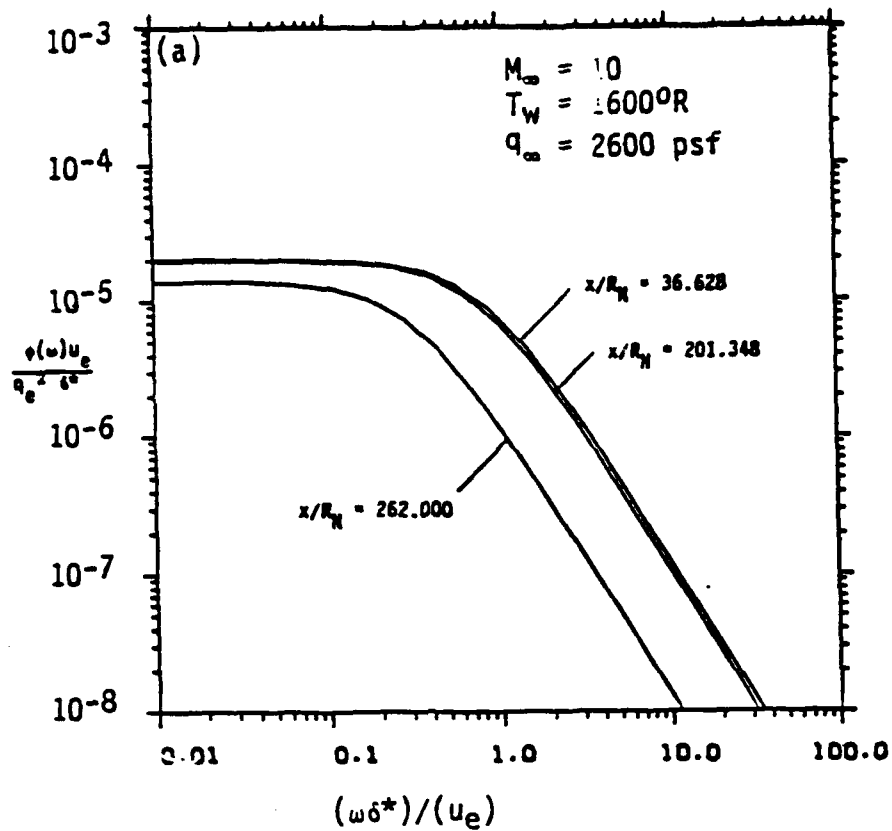


Figure 14. Power Spectra on Windward Meridian of BWB at Mach 10

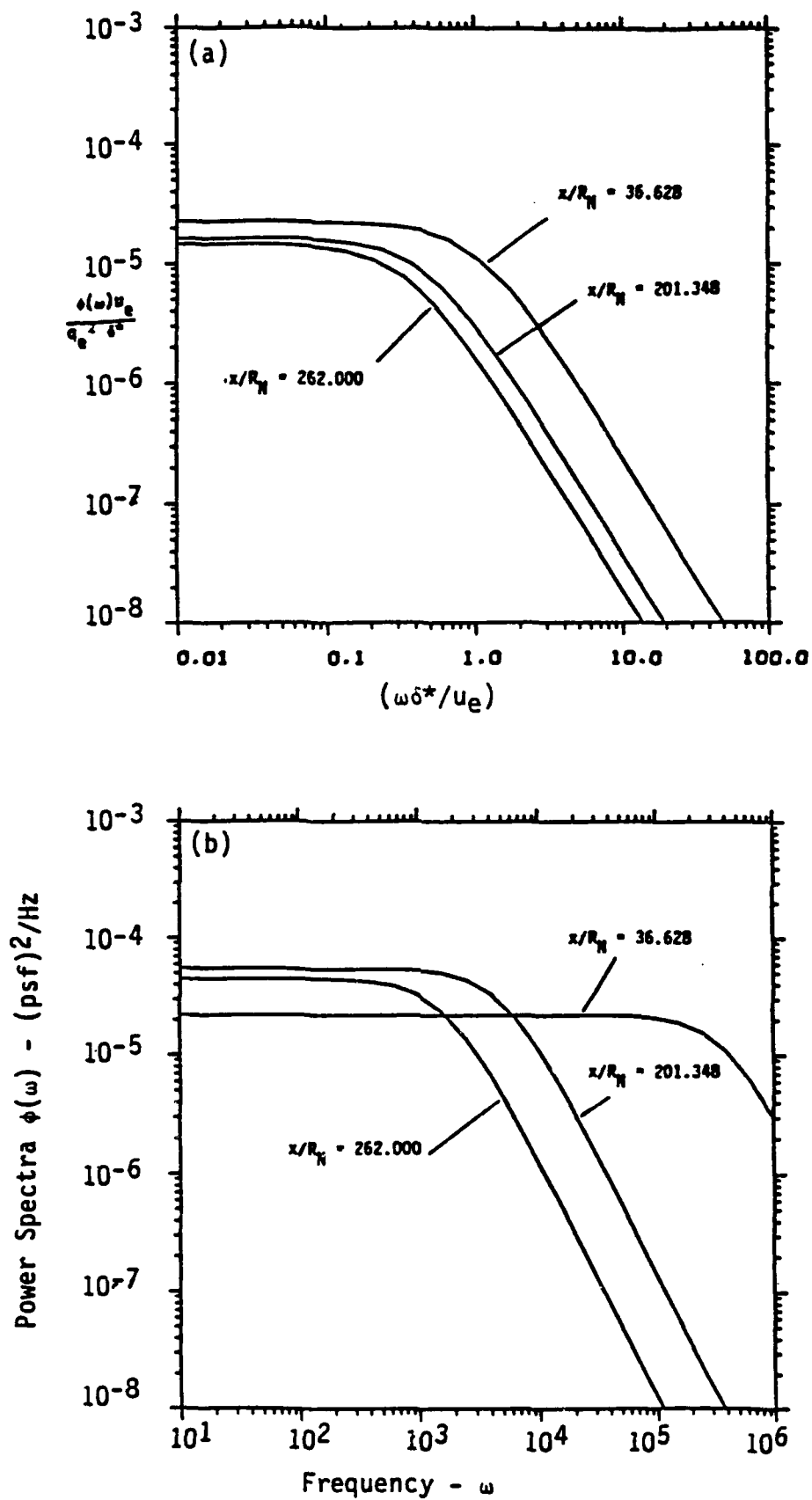


Figure 15. Power Spectra on Leeward Meridian of BWB at Mach 10

potential bow shock interaction with the shock/boundary layer of the HS/VS while the inlet splitter plate is subject to bow shock interactions. The type of interactions that could be generated are shown in Figure (16) and include the following:

- (1) Fin generated: vertical stabilizer shock with aftbody boundary layer ( $x/R_n > 200$ ). Ramp guide-rails and inlet splitter plate with cowl.
- (2) Axial off-set fin: horizontal stabilizer shock with vortical stabilizer boundary layer; consider the offset distance greater than the boundary layer thickness so as to use the swept fin and sharp fin data base.
- (3) Axial corner: offset distance of the order of the boundary layer thickness for both HS/VS shock boundary layer interactions. Ramp guide rails with ramp as well as inlet splitter plate with inlet/cowl.
- (4) Fin generated: bow shock interaction with horizontal stabilizer boundary layer (2D flow). Also bow shock interaction with inlet region.
- (5) Compression corner: second compression ramp on windward side of body.

It was found that the strongest potential interaction involved the bow shock and horizontal stabilizer boundary layer. For this condition, peak rms fluctuating pressure was shown to increase by factors of 30 (30 db) to 240 (48 db) over the approach flow level for free stream Mach numbers between 10 and 20. For the Mach number regime smaller than 10 the interaction of the bow shock/HS boundary layer was not likely due to the wide shock angle. The power spectra was shown to increase by factors  $10^3$  to  $10^4$ . The



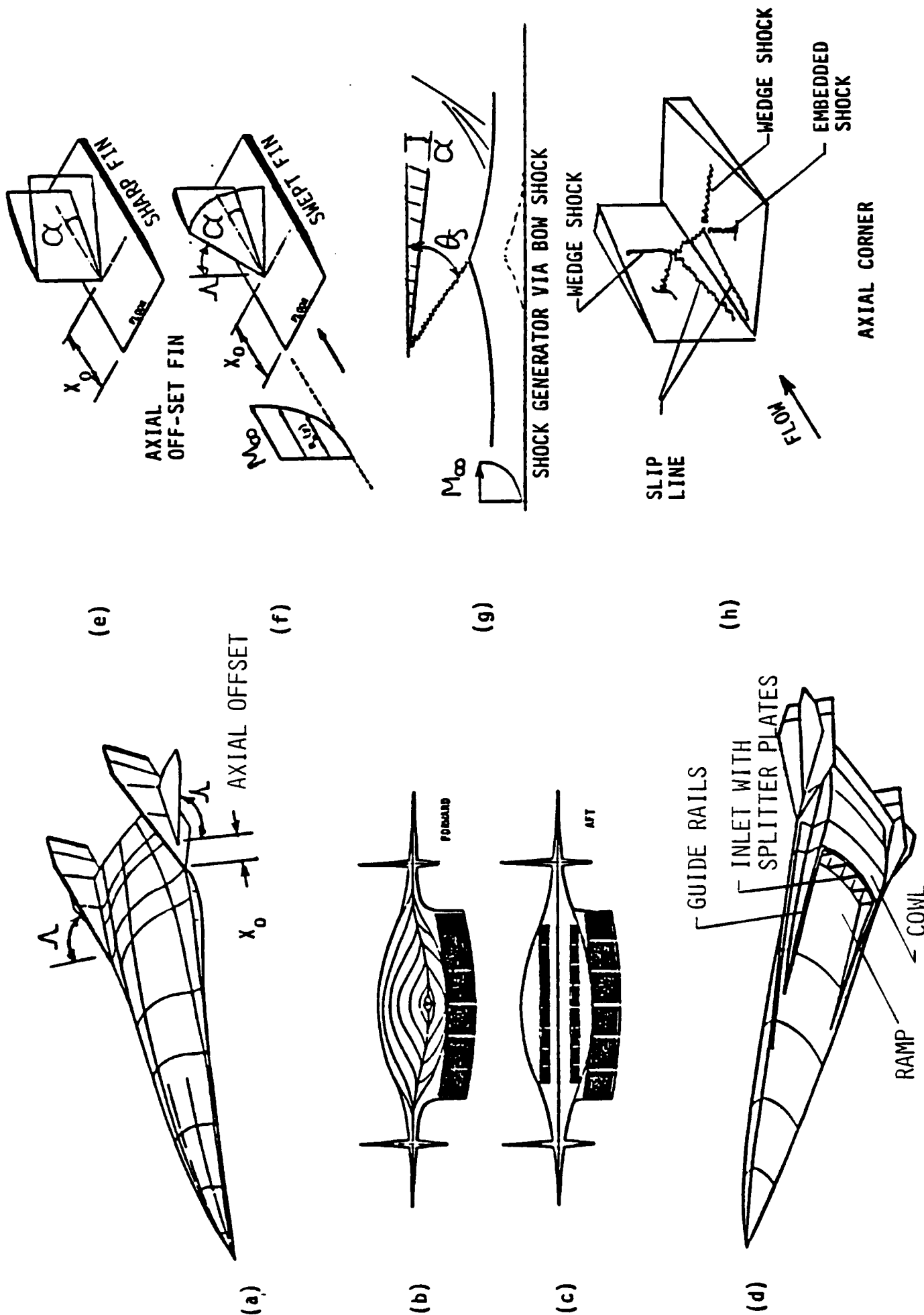


Figure 16. Views of Blended Wing Body (a-d) and Potential Shock/Boundary Layer Interactions (e-h)

impact of the bow shock on the inlet which would produce a shock on shock with a viscous approach flow (ramp) was not investigated.

The low shock generated angles ( $\alpha < 2$  degrees) on the BWB control surfaces (VS/HS) developed a weak interaction that did not impact the approach boundary layer acoustic levels.

The axial corner flow when two surfaces approach a common origin as generated by the HS/VS presents potential interactions. The acoustic loads were shown to be of the order of 3 times the approach flow levels. The axial corner flow developed in the inlet region presents a more complex flow structure whereby shock interactions from the cowl leading edge can interact with the inlet splitter plate and airframe corner flow. Further in integration of this flow region is required.

While References (3) and (22) represent state-of-the-art prediction capability for non-attached flows, a mounting interest in defining aeroacoustic loads is developing for structural design. References (25) and (26) provide experimental work at Mach 3 and Mach 5, respectively. In the former wall pressure fluctuations were investigated in the reattachment region of a free shear layer. It was determined that the reattachment region on a 2D ramp was highly unsteady and provided wall pressure loading similar in scale and magnitude to 2D compression ramp flows at the same Mach number (Reference 13 for example). The work of Reference (26) focused on shock motion in a compression ramp interaction with the approach boundary layer. This investigation was concerned with the large scale structure of the incoming boundary layer to influence the interaction region and is considered more appropriate for fundamental modeling of the turbulence structure.

An excellent experimental investigation of an axial-compression interior-corner region with shock impingement was

recently conducted<sup>27</sup> in the NASA Langley 20-inch Mach 6 Tunnel. The experiment represents a simulation of a hypersonic engine inlet region. The unique feature of the test provided an oblique shock generated by a forebody leading surface that impinged upon a 90° axial compression corner formed by the intersection of the cowl and strut (splitter plate). Although no acoustic data was obtained, the heat transfer results show the complexity of the interacting shock/shock/boundary layer flow and can provide insight to instrumentation location requirements.

Finally, a workshop was recently held at Pratt and Whitney<sup>28</sup> for the purpose of discussing state-of-the-art predictions capability for NASP type configurations; specifically in the areas of heat transfer and aeroacoustic loads. The conclusions reached at this meeting were primarily the same as addressed in Reference (22) and subsequently reiterated and expanded upon in this report. Several new sources of acoustic data were noted, in particular for the inlet/combustion region that could potentially be of value. These data are currently being examined. This data base should be available during the Phase II program. Of particular interest is acoustic data for the combustor in the scram-jet mode.

## 5. Assessment of Literature Review and Prediction Capability

The review has been concerned with the prediction of rms fluctuation pressure and power spectra for attached and separated turbulent boundary layer flow. The technique considered is based both on fluid dynamic principles using the Houbolt algorithm for the power spectra intensity and the experimental data base. Regimes of flow include the attached turbulent flow for both smooth and rough surfaces and the separated flows generated by compression corners or by fin generated shock impingement. Comparison of the predictions with the data base have been adequate.

It was shown that the technique could be applied to a space transportation system (McDonnell-Douglas Blended Wing Body) which presented additional shock/boundary layer interactions of control surfaces and the potential to examine the ramp (viscous flow)/inlet/cowl surface interactions.

While the data base for attached hypersonic turbulent boundary layer flow is not extensive, shock/boundary layer interaction type flow is very limited ( $M < 3$ ). Thus a desirable program to extend the data base of acoustic data for  $M > 3$  and should include the cross power spectra density as well as the rms pressure and power spectra.

The program should include the three dimensional aspect of lifting surfaces flows such as discussed above for the BWB. These are:

- (1) Experiments that include approach flows that are boundary layer (viscous) as well as inviscid with axial corner and axial offset shock generating geometries such as the inlet region and fuselage/stabilizer regions.
- (2) Shock orientation with respect to the boundary layer - simulate the potential bow shock/horizontal stabilizer boundary layer interaction.
- (3) Shock/laminar boundary interactions which are characteristic at the higher Mach number altitudes.
- (4) Shock on shock/boundary layer interactions - bow shock on control surface shock/boundary layer as well as inlet/cowl region interactions.

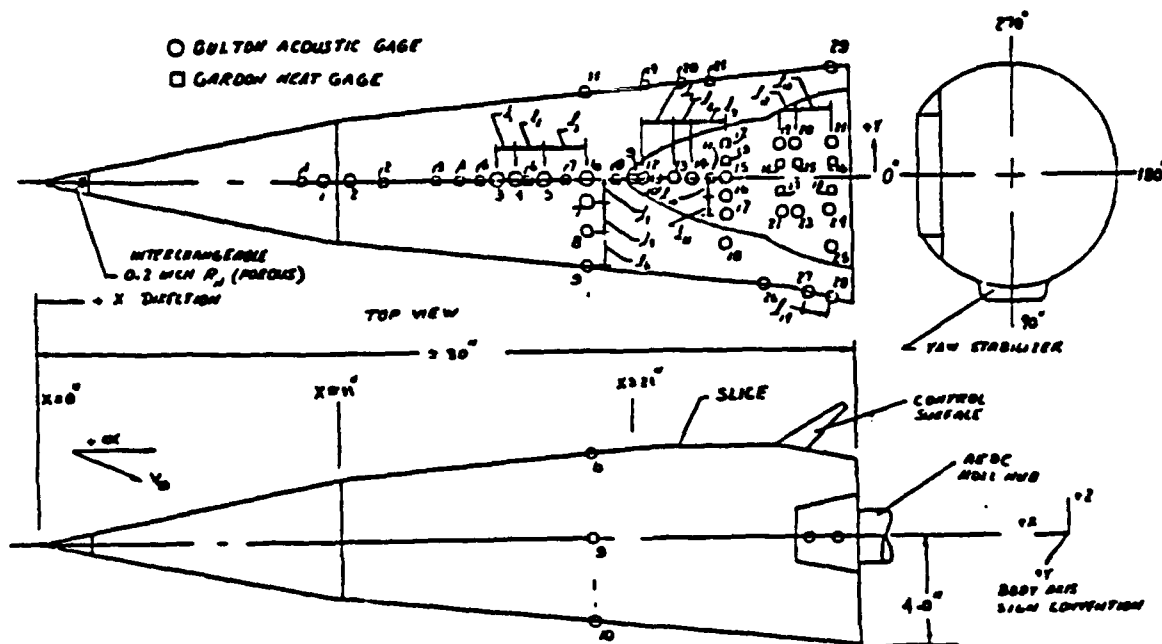
### III EVALUATION OF ATTACHED AND SEPARATED FLOW EXPERIMENTS AT MACH 4 AND MACH 8

#### 1. AEDC MACH 4 AND MACH 8 DATA

An extensive experimental investigation was conducted<sup>2,6</sup> in the Arnold Engineering Development Center's von Karman facility at Mach 4 (Tunnel A) and Mach 8 (Tunnel B). The test models consisted of sphere-cone/slice/flap and a sphere-bicone/slice flap configurations. Figure (17) shows a schematic drawing of the configurations as well as sensor (heat transfer and dynamic pressure) locations. Interchangeable nose tips consisting of sharp and blunt shapes were used. The latter consisted of a porous design in order to provide transpiration gases to control boundary layer transition zones over the model gage arrays. Test conditions were:

$$\begin{aligned} 2.5 \times 10^6 < Re_{\infty}/ft < 3.7 \times 10^6 \\ M_{\infty} &= 4 \text{ and } 8 \\ 0 \leq \alpha \text{ (angle of attack)} &\leq 14^\circ \\ 0 \leq \phi \text{ (yaw)} &\leq 90^\circ \\ 0 \leq \delta_f \text{ (flap deflection)} &\leq 20^\circ \end{aligned}$$

Inasmuch as large flap deflections as well as combined flap deflection and angle of attack could produce flow separation, these data were reevaluated relative to the scaling criteria developed by Laganelli and Wolfe<sup>3</sup>. In particular, the effect of separation onset location on the slice gages was critically examined for increases in rms pressure fluctuation levels over approach flow levels (from the conical region). After considerable review of the processed data it was determined that flow separation apparently did not occur; i.e., no significant rise in rms pressure was observed indicative of shock separation onset or plateau regions as experienced in the 2D Mach 3 experiments shown in Figures (4) and (5).



36

Figures (18) and (19) show the rms fluctuating pressure normalized with the local mean pressure along the cone/slice/flat regions. These results are typical of the experiments of References (2) and (6). The table inset in these figures show the flap deflection angle, angle of attack, bluntness, transition zones, and pressure rise from the slice to flap (maximum level and calculated level). An examination of Figure (18) (Mach 4) clearly does not show any effect of a separation region relative to rms pressure rise. However, one notes the impact of transition region. For example, along the conical region an increase of a factor of 3 is shown for those gages immersed in the transition region. On the other hand, the blunt nose (with blowing which creates early transition) and the angle of attack cases reflect turbulent levels experienced in other tests. The gages showing the higher rms levels carry the turbulence scale (approach flow) through the flow expansion region of the cone/slice and are shown to be at higher levels. Relative to the flap region, normalizing by the local mean pressure should also provide a consistent distribution, i.e., where the effect of  $\delta_f$  and  $\alpha$  are scaled by pressure. However case 102 (blunt non-blowing nose tip) had a transition zone that extended to the flap and resulted in much higher dynamic pressure levels. Also, the predicted pressure rise is shown to be more than the maximum inviscid pressure rise which implies a potential error in the mean pressure data. The higher level of case 103 along the flap (blunt with blowing) could reflect the same problem.

The Mach 8 case (Figure 19) presents a much more complex situation. For these tests, the end of transition was nominally between 20 and 25 inches which would imply that the conical gages were in the transition regime while the slice/flap region was subject to non-equilibrium flow conditions and possible separation. Relative to separation, the gage location at the axial distance of 28 inches shows a rise over the upstream position (26.5 inches) which is generally higher than the normalized flap measured dynamic

# CONE/SLICE/FLAP

MINF=4 REINF/FT=3.6X10<sup>-6</sup>

| SYMBOL | RUN# | Rn | delta | Xtro | Xtre | (Pwf/Pws)max | (Pwf/Pws)calc |
|--------|------|----|-------|------|------|--------------|---------------|
| □      | 6    | 0  | 0     | 15   | 24   | 2.45         | 2.06          |
| △      | 23   | 0  | 7     | 15   | 24   | 4.69         | 3.85          |
| ◇      | 27   | 0  | 15    | 15   | 24   | 4.07         | 4.80          |
| ○      | 102  | .4 | 20    | 20   | 30   | 5.02         | 4.80          |
| ◇      | 103  | .4 | 20    | 20   | 6    | 6.33         | 5.30          |
| ◇      | 42   | 0  | 20    | 15   | 24   | -            | -             |
| ◇      | 90   | .4 | 0     | 0    | 0    | 3.74         | 1.85          |
| △      | 25   | 0  | 7     | 15   | 23   | 5.78         | 3.34          |
| x      | 30   | 0  | 15    | 15   | 23   | -            | -             |

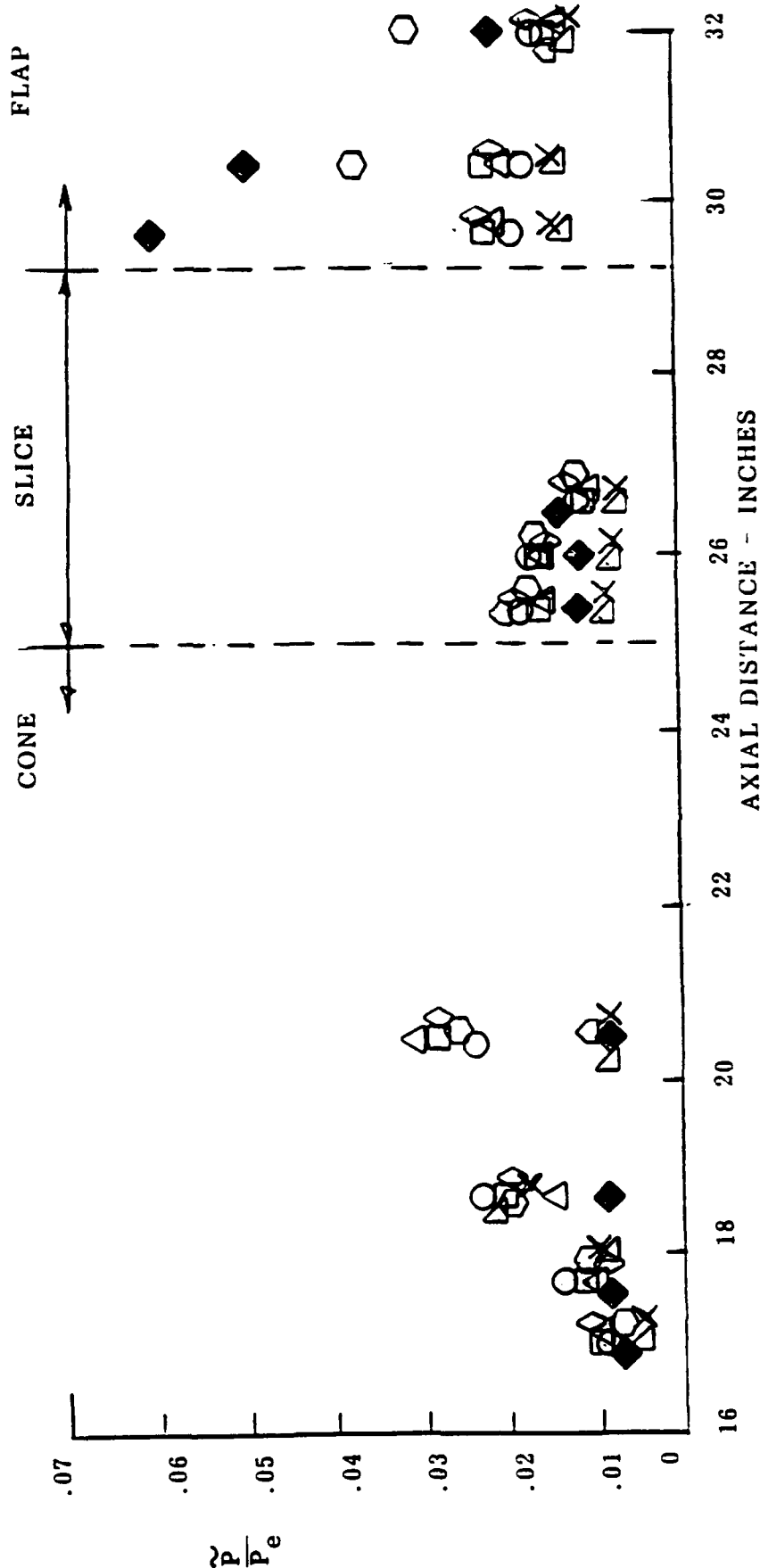


Figure 18. RMS Pressure Distribution With Local Surface Pressure at Mach 4



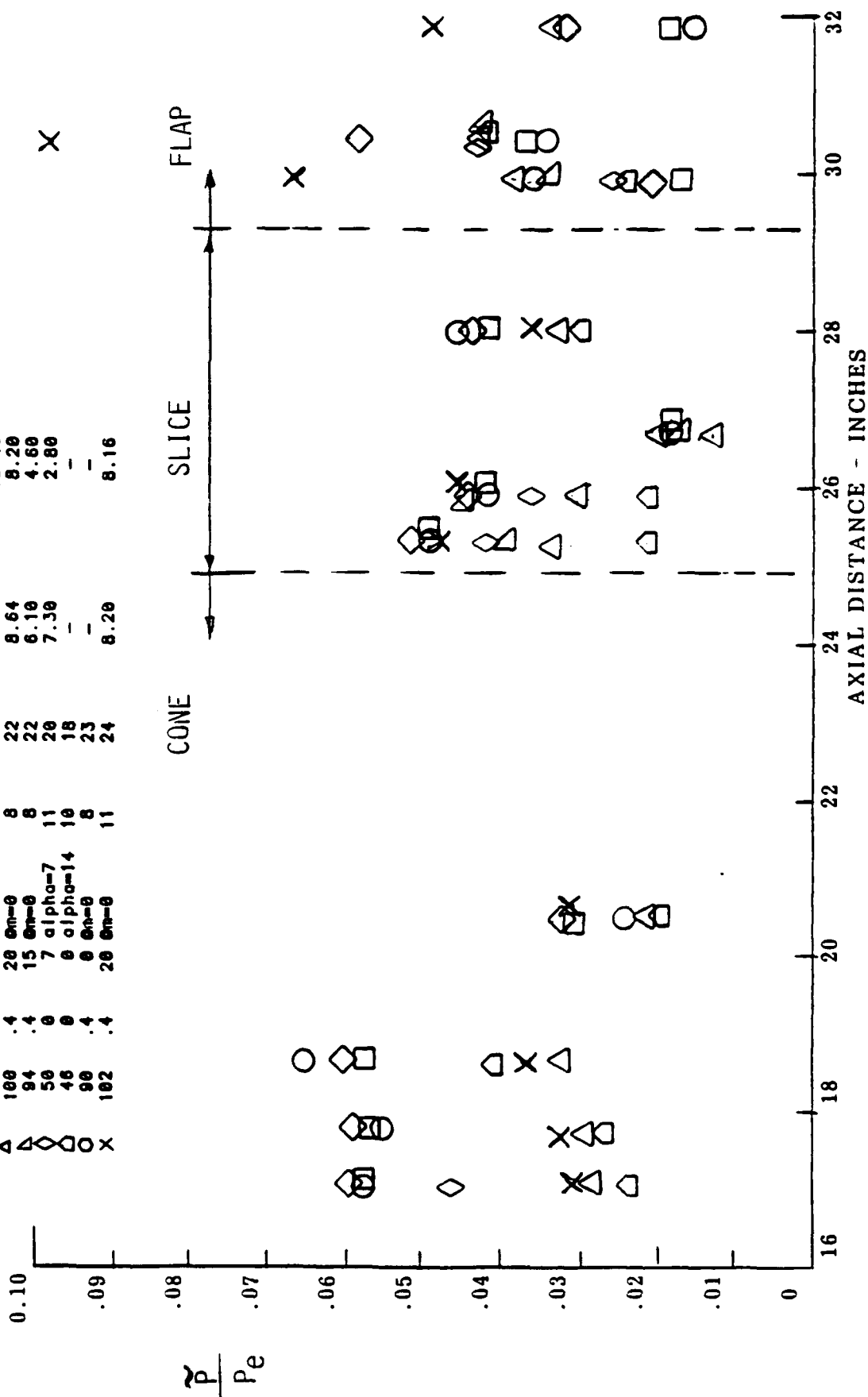
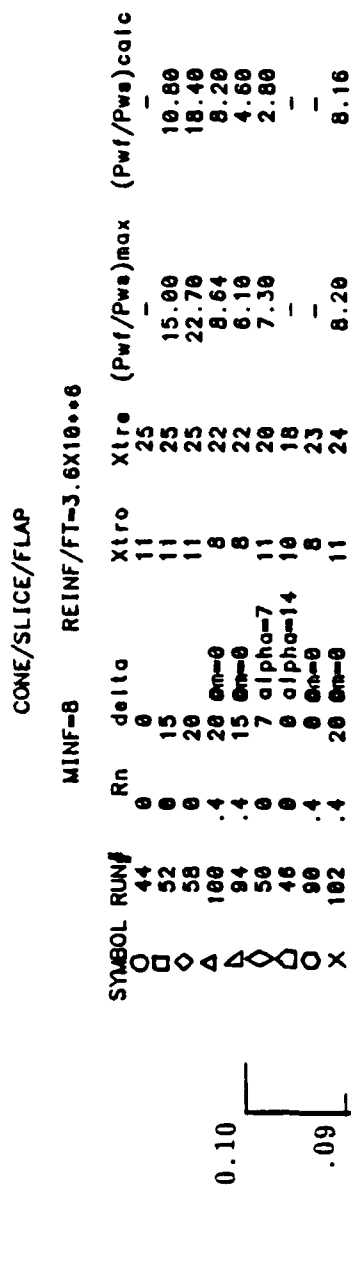


Figure 19. RMS Pressure Distribution With Local Surface Pressure at Mach 8

pressures except for case 102. An examination of the table inset shows that the predicted pressure rise is less than the maximum inviscid pressure rise, except for case 102 (other blunt nose cases show higher predicted values), and maybe a result of possible errors in predictions. It should be noted that an integral boundary layer code was used for the calculations that used correlations for boundary layer growth due to mass transfer. The wide spread in the data along the slice/flap regions makes the interpretation of the data very difficult. The next section will provide some insight to this phenomenon.

## 2. Assessment of the AEDC Mach 4 and 8 Data Base

There are several fluid flow phenomena that are believed to contribute to the observed variation in rms pressure fluctuations along the cone/slice/flap configuration. These include transition, non-equilibrium turbulence effects (which occurs downstream of transition), 3D pressure relief, flow expansion (cone/slice), flow compression (slice/flap), compressibility (reduces the size of the boundary layer), wave cancellation (expansion waves mitigating the compression waves), and entropy effects (bluntness).

Transition is known to produce rms fluctuating pressure levels that are greater than turbulent boundary layer levels. An extensive literature base is available that describes the transition process, where instability of the flow produces large scale turbulence which is the likely phenomenon creating the increased dynamic pressure (especially in the low frequency regime  $<2000$  HZ). The effect of non-equilibrium flow on dynamic pressure has not been investigated, per se, to the authors knowledge. Intuitively, one would not expect a significant impact inasmuch as measured heat flux and wall shear in this region do not show large departures from equilibrium (fully developed similar) boundary layer flow. An examination of Equations (1) and (4) shows that for  $n < 7$  (similar

flow), the dynamic pressure will increase. Measurements in compressible transitional flow have been shown to be in the range  $2 < n < 7$  while in the non-equilibrium region the velocity power law exponent is in the range  $7 < n < 16$ . Using values of  $2 \leq n \leq 6$  can increase the rms pressure by a factor of 3. On the other hand, for values of  $7 < n < 16$ , a variation of less than 25% would occur.

The effect of 3D pressure gradients (pressure relief) can have a significant effect on the measured dynamic pressure. Figure (20) shows the cone/slice/flap configuration with the pattern of 2D, axi-symmetric, and 3D flow stream lines. As noted, a divergence of the streamlines occur from the 2D planar flows to the 3D flows experienced by the configuration tested at AEDC. This discussion is presented since the codes used in the experimental investigation of References (2) and (6) were 2D planar and axisymmetric. Use of 3D parabolized Navier-Stokes (PNS) solutions (especially at angle of attack) have shown that 2D codes cannot model important 3D effects. Hence, gages located off the main meridian will experience pressure relief which attenuates the rms pressure level. Further discussion of Figure (20) will be given below.

The curved bow shock occurring on a blunt nosetip produces a vortical flowfield which is a source in the production of turbulence. This vorticity should enhance the dynamic pressure levels, and when coupled with other flow phenomena such as transition and non-equilibrium, can augment the power intensity to higher levels. This was experienced at both the Mach 4 and Mach 8 test conditions (blunt nose cases). The phenomenon can be further complicated when subject to compressibility (i.e., Mach 8 compared to Mach 4) which tends to reduce the size of the boundary layer and impact the effect of the scale lengths in the low frequency regime. Moreover, the effect of compressibility tends to bring the sonic line closer to the wall and subsequently retards separation potential, or at least restricts the separation zone to a very

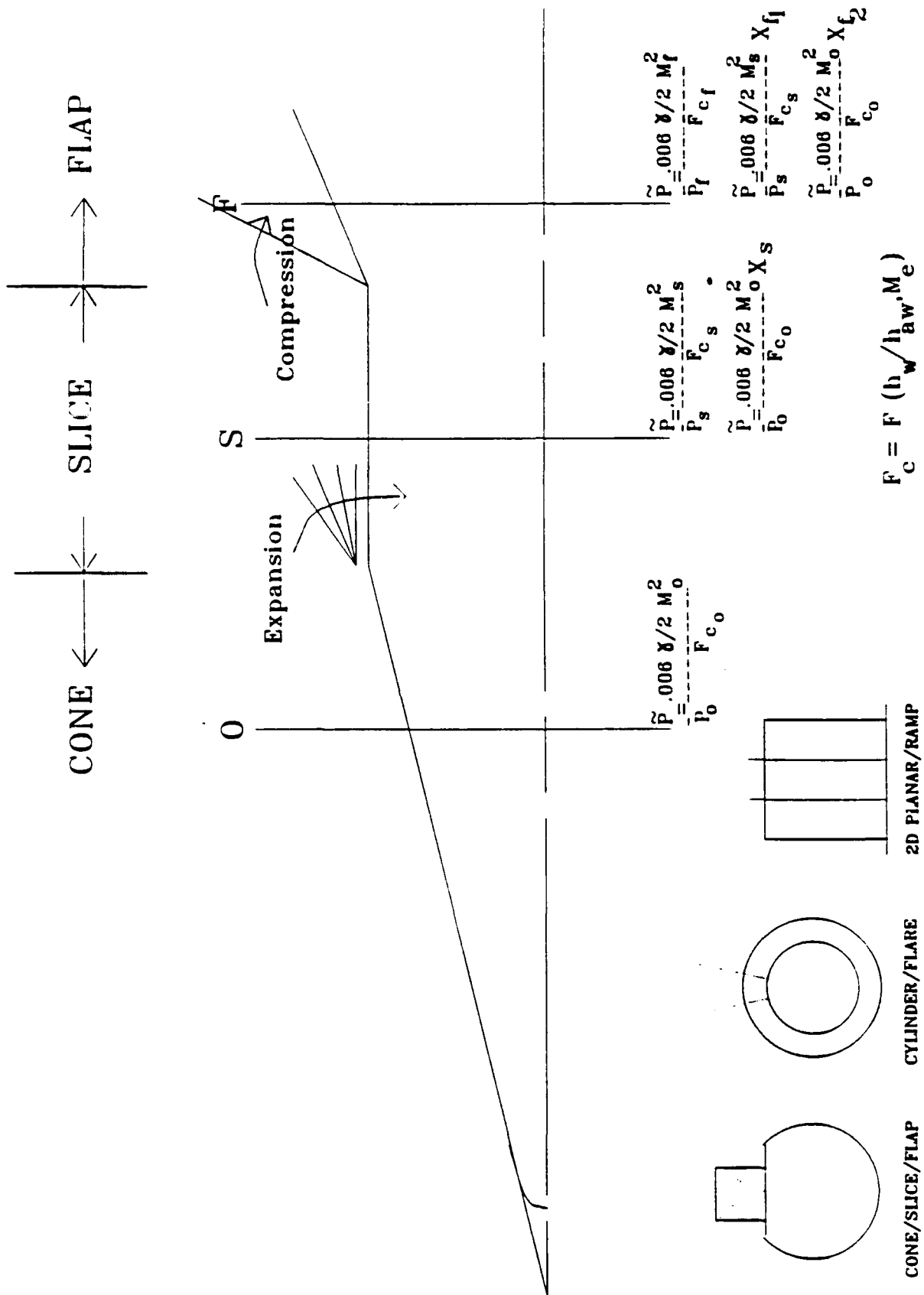


Figure 20. Typical Cone-Slice-Flap Configuration with Streamline Spreading

small region at the compression corner. Further discussion concerning this phenomena will follow.

An examination of Figures (17) and (20) shows that the slice region is approximately the same length as the flap region (about 4.5 inches). The expansion waves developed from the cone/slice could impact the compression waves developed from the slice/flap corner potentially weakening the compression wave; hence suppressing the strength of the interaction and the potential of flow separation. The length of the slice region would appear to play a major role in this interaction. Also, as previously noted, the effect of entropy which produces vorticity will attenuate the dynamic pressure by expansion while augmenting the dynamic pressure through compression.

In an attempt to understand these fluid dynamic phenomena, the SAIC SCRAMP<sup>29</sup> (3D PNS) code was exercised for the cone/slice/flap configuration. Figures (21) and (22) show these results at Mach 4 and Mach 8, respectively. Figure (21A) shows a typical blunt nose case with a 15° flap at zero angle of attack. The pressure contour levels represent pressure ratio of local to free stream values from the body to bow shock. The compression shock is shown over the flap region where high pressure contours are expected (purple), a zone of mild pressure (red,  $P_w/P_\infty < 1$ ) is noted between the compression shock and the expansion wave (yellow, emanating from the cone/slice junction). An inviscid region exists from the expansion wave (green) to the bow shock (top yellow). For this situation, the expansion wave could potentially influence the region over the flap; but does not interact with the compression shock. At angle of attack (Figure 21B) the pressure contours are stronger on the flap as expected and the expansion wave is blending into the inviscid region. Figure (21C) provides an assessment of the expansion wave effect. Here, the slice region was artificially made four times the length as that shown in Figure 21A. For this

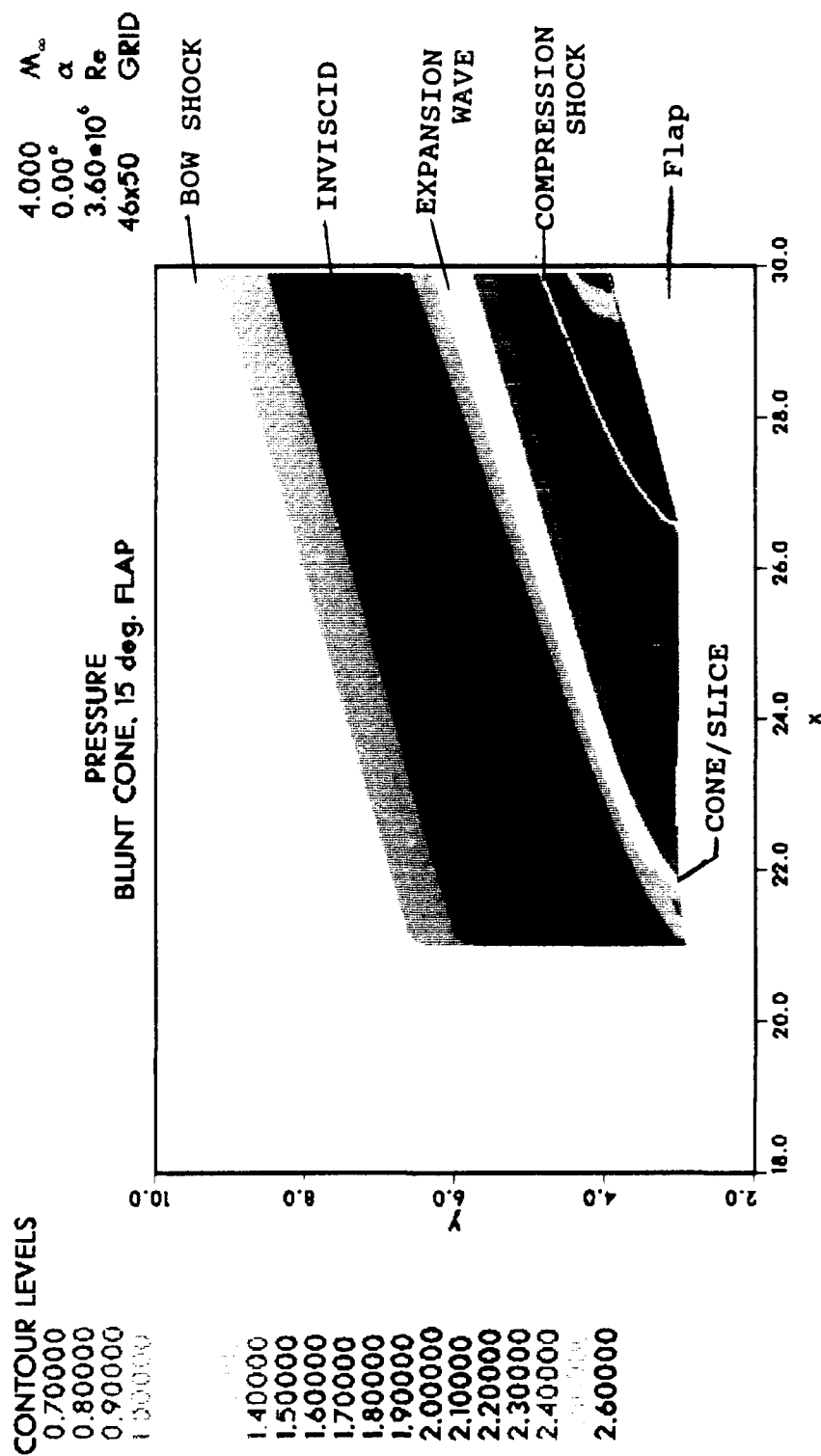


Figure 21A. PNS Solutions of Pressure Contours on Blunt Cone  
with 15° Flap at Mach 4

1.00000  
1.20000  
1.40000

2.200000  
2.400000  
2.600000  
2.800000  
3.000000  
3.200000  
3.400000  
3.600000  
3.800000  
4.000000

4.000  $M_{\odot}$   
7.00°  $\alpha$   
3.60•10<sup>6</sup> R<sub>☉</sub>  
25x50 GRID

**PRESSURE  
BLUNT CONE. 15 deg. FLAP**

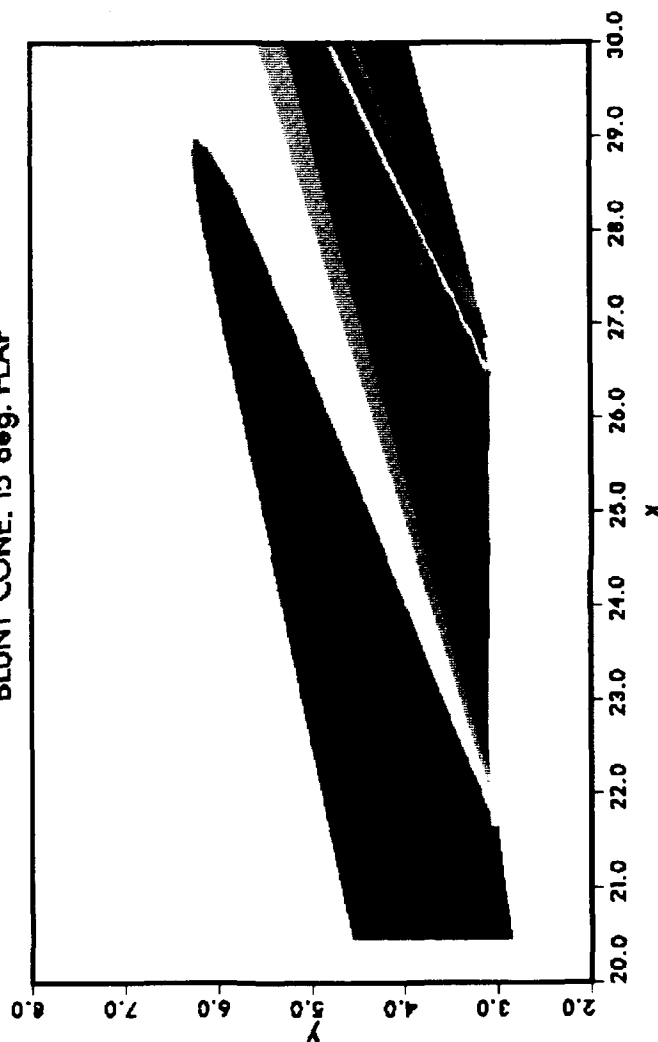


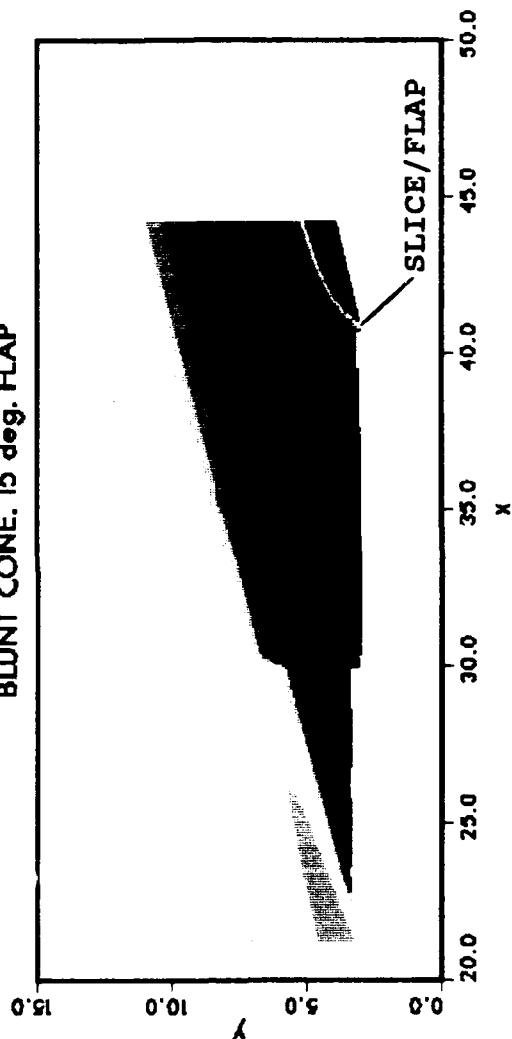
**Figure 21B. PNS Solutions of Pressure Contours on Blunt Cone with 15° Flap at Mach 4**

CONTOUR LEVELS

0.70000  
0.80000  
0.90000  
1.00000  
1.10000

1.60000  
1.70000  
1.80000  
1.90000  
2.00000  
2.10000  
2.20000  
2.30000  
2.40000  
2.50000  
2.60000  
2.70000  
2.80000  
2.90000  
3.00000  
3.10000  
3.20000

PRESSURE  
BLUNT CONE. 15 deg. FLAP



4.000  $M_\infty$   
0.00°  $\alpha$   
3.60e10<sup>4</sup>  $Re$   
58x50 GRID

Figure 21C. PNS Solutions of Pressure Contours on Blunt Cone with 15° Flap at Mach 4



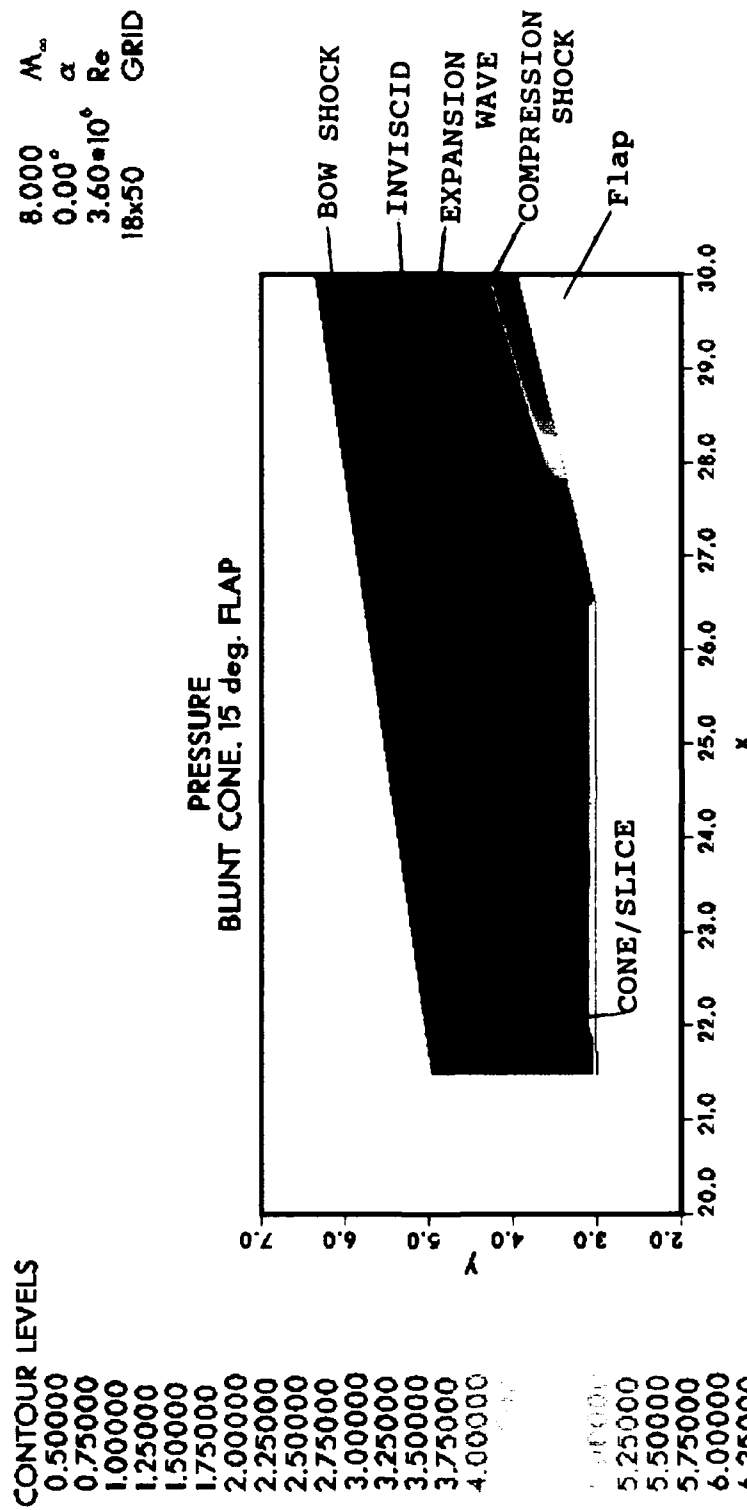


Figure 22A. PNS Solutions of Pressure Contours on Blunt Cone  
 with 15° Flap at Mach 8

## CONTOUR LEVELS

1.00000  
1.50000  
2.00000  
2.50000  
3.00000  
3.50000  
4.00000  
4.50000  
5.00000  
5.50000  
6.00000  
6.50000  
7.00000  
7.50000  
8.00000  
8.50000

11.5000  
12.0000  
12.5000  
13.0000  
13.5000  
14.0000  
14.5000  
15.0000  
15.5000  
16.0000

8.000  $M_\infty$   
7.00°  $\alpha$   
3.60e10° Re  
19x50 GRID

PRESSURE  
BLUNT CONE, 15 deg. FLAP

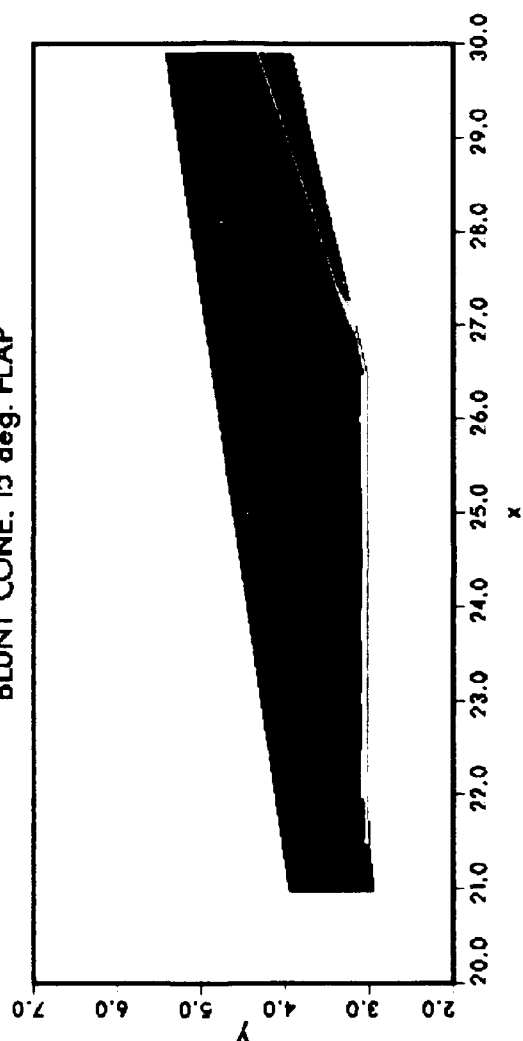


Figure 22B. PNS Solutions of Pressure Contours on Blunt Cone  
with 15° Flap at Mach 8

situation, the expansion wave is enveloped into the inviscid region close to the bow shock and has no effect on the flap region. Shortening the slice region would promote expansion/compression shock interaction.

Figure (22) shows the pressure contours at Mach 8 for a blunt nosetip with/without angle of attack. The same process is occurring and the effect of compressibility to shrink the inviscid and viscous regions are noted. It is interesting to observe the pressure distribution along the flap (zero angle of attack) compared to the Mach 4 case. Here, a more extensive zone of lower pressure is shown from the compression corner. The expansion wave as in the Mach 4 case does not interact with the compression shock. As expected, angle of attack provides an increase in pressure on the flap region.

A review of experiments featuring flow separation due to compression corners has shown that the shock generating ramp is usually high ( $>15^\circ$ ) and the approach boundary layer flow was significant ( $\delta > 3$  inches). In the present investigation, the approach flow boundary layer was less than one inch and the shock generating flap angles less than  $20^\circ$ . When the boundary layer is sufficiently large (i.e., on the order of 3 to 5 inches), the sonic line will also be a sufficient distance from the surface where subsonic flow can circulate upstream during separation. A measure of the ratio of the height of the sonic line was shown to be approximately 0.05. Hence, for a 4 inch thick boundary layer, the sonic line could be 0.20 inches from the wall.

Figure (23) was structured to illustrate the Mach number profiles for the cone/slice/flap configuration using the SAIC SCRAMP 3D PNS code. One notes that the ratio of  $\delta_{M=1}/\delta_{M_e}$  is on the order of the compression corner experiments (i.e.,  $\approx 0.05$ ). However, with the smaller approach flow boundary layer thickness,



the region of incompressible flow is shown to be less than 0.02 inches for both the Mach 4 and Mach 8 tests. It is believed that this suppressed layer does not allow for separation to occur or keeps the potential of separation close to the compression corner.

#### IV EXPERIMENTAL PLAN

##### 1. Introduction/Problem Definition

The high temperatures and fluctuating pressures experienced in hypersonic turbulent boundary layers are known to impact vehicle structures, equipment stations, and crew compartments. Moreover, lifting body designs required for space transportation systems featuring control surfaces can generate higher sound pressure levels as a result of the increased static pressure levels and flow separation. The latter phenomenon can be developed in adverse pressure gradient regions associated with ramp type flows and shock/boundary layer interactions as generated by a bow shock/fin (stabilizer), cowl leading edge and other control mechanisms.

The resolution of these design problems has relied on experimental data where empirical models have been developed to predict the aeroacoustic loads on supersonic/hypersonic structures. The data base that has been generated has focused on attached boundary layer type flow over a reasonable Mach number range. However, the data base is seriously lacking for flows featuring shock/boundary layer interactions in supersonic flows ( $M > 3$ ), and is virtually non-existent for hypersonic flows ( $M > 6$ ). Figure (16) shows a typical design of an air-breathing space transportation system that would experience several types of attached and non-attached flow interaction regions. These regions consist of the horizontal/vertical stabilizers (HS/VS), the VS with the aftbody fuselage, bow shock/HS, ramp (compression), and inlet. The types of interactions are represented in Figures 16-e through 16-h by

potential shock/boundary interactions investigated in the literature.

The types of interactions previously described include:

- (1) Fin generated: vertical stabilizer shock with aftbody boundary.
- (2) Axial offset fin: horizontal stabilizer shock with vertical stabilizer boundary layer
- (3) Axial corner: both HS/VS shock-boundary layer interaction where  $X_0 \sim O(\delta)$ . While cowl inlet represents a classic axial corner flow, the impact of the distance  $X_0$  for the stabilizers has never been treated.
- (4) Fin generated: bow shock interaction with horizontal stabilizer boundary layer (2D flow).
- (5) Compression corner: compression ramp on windward side of body.
- (6) Combinations of the above interactions such as bow shock/cowl inlet shock interactions with ramp boundary layer approach flow.

The characteristics of swept shock/boundary layer interactions propagating from spanwise inboard corner boundary conditions has been investigated by Settles and Dolling (Reference 30) as well as Inger (Reference 31) of which the interactions shown in Figure (16) represent a sub-set. Fin generated shock/boundary layer interactions represent a class of 2D and 3D flows for which  $X_0 \gg \delta_0$ . Pressure (rms and mean), profile, and heat transfer data have been obtained for this type of interaction. The rms pressure has

generally been restricted in Mach number ( $M \leq 3$ ) while mean pressure and heat flux data are available over a wider Mach number range.

The axial offset fin represents a potential new class of interaction<sup>32</sup> relative to the offset distance ( $X_0$ ), compared to the boundary layer thickness developed over the distance  $X_0$  (ie.,  $X_0 \sim 0$  ( $\delta$ )). For this condition, the shock/boundary layer interaction could behave as an axial corner flow in one limit ( $X_0 \rightarrow 0$ ) to the sharp/swept fin interaction limit  $X_0 \gg \delta$ . No rms pressure data exists for this condition. Moreover, to the authors best knowledge, the sensitivity of  $X_0$  on mean flow characteristics (pressure/heat transfer) does not exist. The horizontal/vertical stabilizer could potentially be subject to an axial offset shock/boundary layer interaction for which no information is known.

Finally, the axial corner ( $X_0 = 0$ ) shock/boundary layer interaction, while investigated for mean flow (pressure/heat transfer) behavior,<sup>25,33</sup> has no available rms pressure data base. In the axial offset and axial corner shock/boundary layer interaction studies, the approach flow has been inviscid as opposed to a boundary layer flow. The impact of a variable Mach number ( $M = M(y)$ ), on the shock strength and subsequent interaction further complicates the predictive capability of aeroacoustic loads.

## 2. Purpose and Objective of Wind Tunnel Program

The objective of the wind tunnel test program is to extend and/or provide a data base for rms and mean pressure for flows featuring shock/boundary layer interactions; in particular for  $M > 3$ . The test program will focus on the shock/boundary layer interactions of axial, axial-offset, and corner flow configurations. The test program is proposed to be conducted in the WRDC Mach 3 wind tunnel and in the 20 inch hypersonic wind tunnel (20 HWT) at Mach 12. The Mach 3 tests will extend the data base to include

axial offset data (rms and mean pressure) as well as corner flow data (rms pressure). The Mach 12 test will provide an extension to the data base for conditions at  $M > 3$ .

The final result of the test program will be the display of processed data, in graphical and tabular format, which will be suitable for direct use for validation and/or aeroacoustic algorithm development.

### 3. Test Hardware

#### 3.1 Test Model

The test model that will be used in the proposed experimental program consists of a flat plate with a variable angled wedge to provide shock/boundary layer interactions. The model will be designed to allow for an examination of the axial-offset characteristics as well as corner flow behavior. The wall thickness will be selected to minimize vibration while accommodating a wall surface gage. The model will be instrumented with mean (static) and fluctuating (rms) pressure gages. The number of gages selected will be determined in the Phase II Experimental Test Report. A schematic diagram of the proposed model and potential sensor locations for the Mach 3 tests is shown in Figure (24).

The test model will be positioned between the two side walls of the WRDC Mach 3 facility. Several locations can be selected (i.e., between stations 1 and 8); however, previous experience has shown that the location between station 1 and station 3 would be preferable. Essentially, the model will be modular to include small sections that consist of the primary instrumented section and shock generating wedge, a sharp leading edge, and several forebody sections to accommodate the axial offset investigation. The primary section will include a circular disc ( $D < 5"$ ) that will



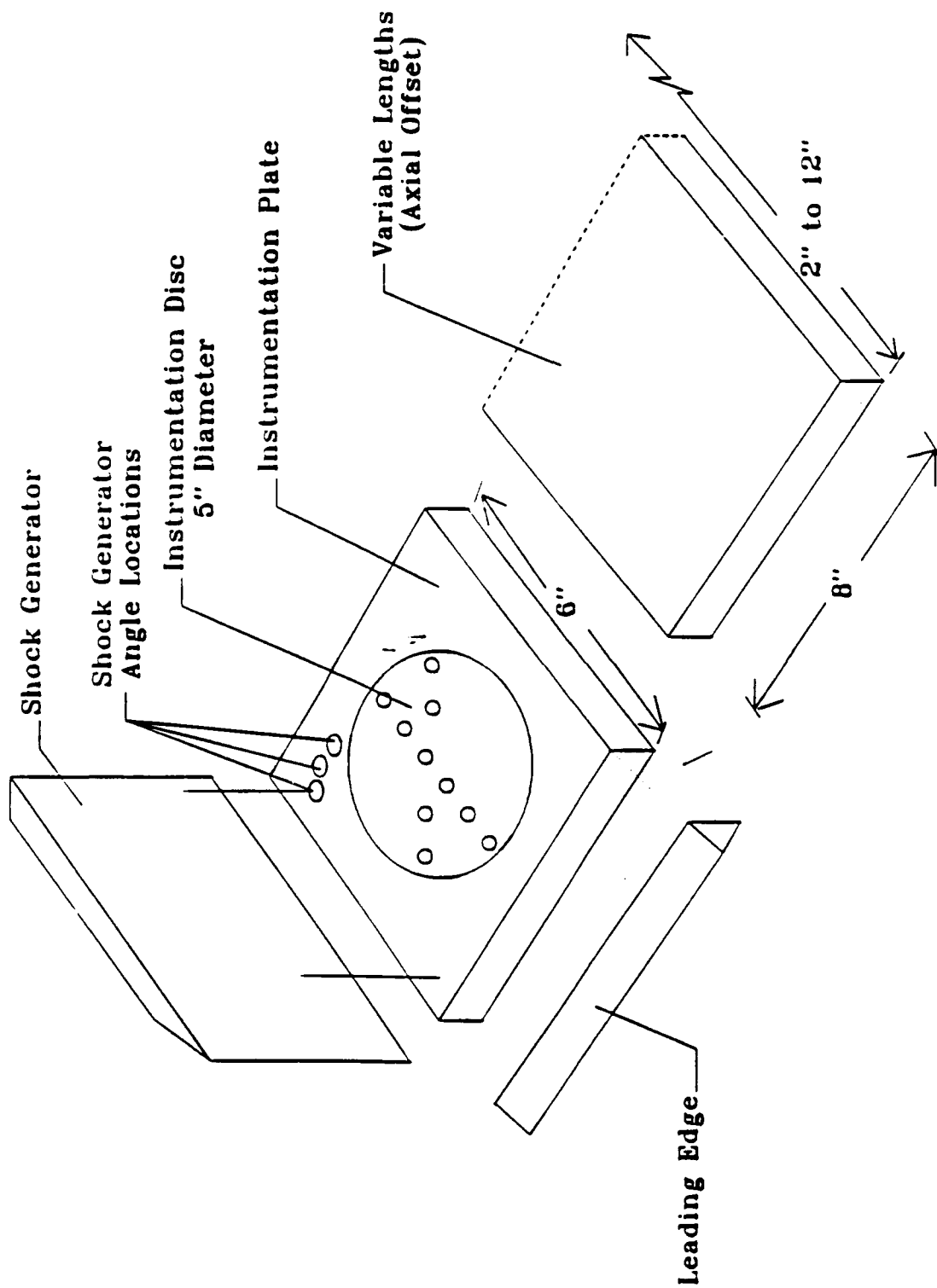


Figure 24. WRDC Mach 3 Facility Test Model

contain the instrumentation. The design will allow the disc to be rotated in order to locate the surface sensors in the interaction region. Both analysis and preliminary tests will help to define the optimum gage locations. Boundary layer transition will not be an issue in the high Reynolds number facility inasmuch as the flow has been determined to be turbulent from the nozzle throat.

#### 4. Instrumentation

Both mean (static) and dynamic (rms) pressure will be measured. Mean pressure data can be obtained by conventional ported-hole designs or as an element in piezoresistive sensors (such as a Kulite differential gage). The dynamic pressure will be measured by acoustic sensors of either the piezoelectric (Gulton type) or piezoresistive (Kulite or PCB) type. The gage selection will be determined based on size and range of sensitivity in order to minimize gage size corrections relative to boundary layer scale factors. In order to maximize signal-to-noise ratio of the acoustic data, an amplification package will be investigated as well as its location (i.e., near the model or external to the tunnel) to drive the signal to an overall level as close as possible to the tape recorder full-scale dynamic range available. Auto-Gain Amplifiers will be used to filter any selected combinations of sensor signals using a 6db/octave, selectable low-frequency cut-off capability to compensate for the severe high frequency attenuation due to the shock/boundary layer interaction in order to contain the full spectral response of the gage within the designed dynamic range.

The data will be recorded on a Honeywell Portable Signal/Condition/Amplifier (or equivalent) that features a built-in calibration routine. The signal will also be monitored with oscilloscopes for real-time assessment of the flow behavior. The quick-look data evaluation can be made with the Honeywell dynamic

signal analyzer which incorporates a built-in plotting function with graphical display. This methodology will be used to determine gage location (disc rotation) as a guide to subsequent test procedures.

Once a favorable position has been established, flow diagnostics that include shadowgraph, laser doppler (LDV), and surface oil (photography of wall shear and flow directions) can be obtained. The availability and adequacy of these techniques will be investigated. Also the use of temperature sensitive paint (phase change paint technique) will be investigated which can be used simultaneously with infrared photography. The combination of the two techniques can provide heat transfer and wall temperature. These techniques are readily adaptable to the Mach 3 facility which incorporates portal windows on all four walls of the tunnel. The model can be illuminated with stroboscopic lights that will be synchronized with a 35mm color camera to capture the complex shock/boundary interactions which will further provide proper locations for the mean and dynamic pressure gages.

## 5. Test Matrix

Testing will be conducted in the WRDC Mach 3 and 20 inch HWT (Mach 12) facilities. The tests will commence in the Mach 3 facility in order to investigate the axial-offset problem. Pending the results of this investigation, an experimental program will be recommended for the Mach 12 conditions. If the axial-offset problem can be characterized with existing data, i.e., the effect of the boundary layer growth relative the separation distance between two shock generating surfaces, the Mach 12 tests will focus an inviscid and viscous approach flow behavior, as well as flow diagnostic techniques described above. If the axial-offset problem is deemed a potential interaction problem, the Mach 12 tests will require further investigation of this problem. The reason for the

viscous approach flow leading to the interaction surfaces is due to the actual behavior of the flow that is experienced on an airbreathing configuration. For example, the boundary layer flow on the ramp leading into the cowl area (Figure 16) is viscous with a variable Mach number. Three-dimensional shock/boundary layer interactions that have been investigated in the literature have been essentially inviscid hence requiring a proper interpretation to apply experimental results to actual flight conditions. The 20 inch HWT facility provides a thick boundary layer (on the order of 5 inches) at the exit of the nozzle which allows the required test conditions for this behavior. An extension to the nozzle will be designed to include the test model as shown in Figure (25).

Table 4.1 lists the tunnel performance capabilities for the free stream Mach numbers proposed in these tests. It should be noted that the flowfields of those two facilities have been extensively investigated in recent investigations by SAIC References 34 and 35). A test matrix will be developed in the Phase II Experimental Test Report that will reflect the coupling between the aerodynamic and acoustic fields. Both the approach flow and the interaction flowfield will be investigated in order to derive similarity laws relating the two flowfields. The following geometric, flow field, and acoustic parameters will be considered:

**TABLE 4.1 TUNNEL PERFORMANCE CONDITIONS**

| MACH NO. | $p^{\circ}$<br>(psi) | $T^{\circ}$<br>(°R) | $R_{\infty} \times 10^6/\text{ft}$ |
|----------|----------------------|---------------------|------------------------------------|
| 3        | 85                   | 460                 | 44                                 |
| 3        | 240                  | 460                 | 120                                |
| 3        | 400                  | 460                 | 196                                |
| 3        | 560                  | 460                 | 270                                |
| 12       | 600-1200             | 1900                | 0.75                               |

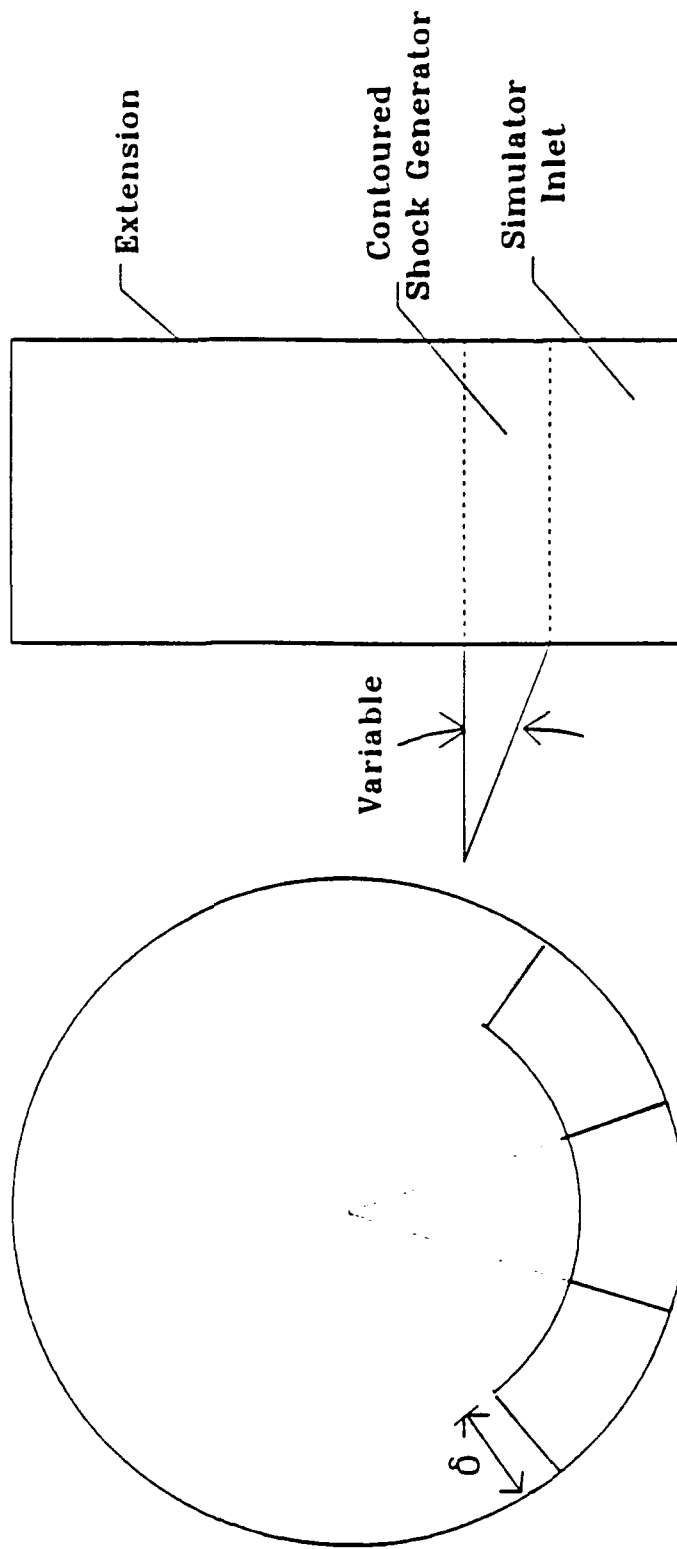
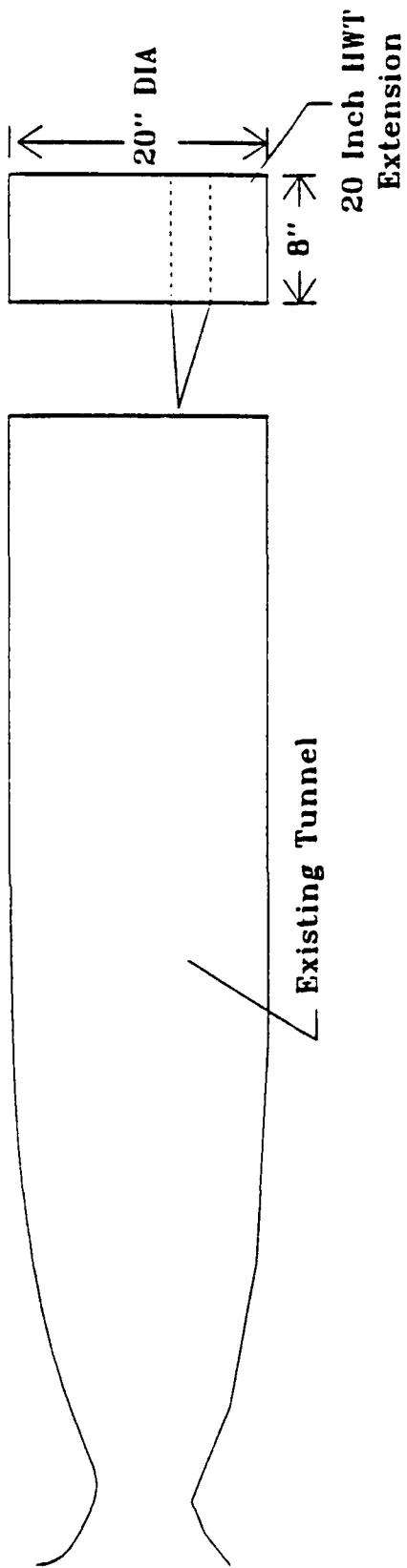


Figure 25. WRDC Mach 12 Facility Test Model

Mach number: 3 and 12  
Pressure (Reynolds number)  
Axial-offset length  
Shock generator angle  
Approach flow (inviscid and viscous)  
RMS and static pressure  
Power spectra and cross-power spectra  
Wall temperature  
Flow diagnostics (pending adaptability)  
Infrared photography  
Phase change paint technique  
Shadowgraph  
Oil flow streamline technique  
Laser velocimeter

Tunnels conditions and data acquisition will be provided by WRDC, including acoustic data processing. SAIC flowfield and viscous interaction codes will be used to evaluate local boundary layer properties from free stream conditions. The data will be assembled in a suitable format for use in developing or validating prediction algorithms, as well as for dissemination to the government and scientific community.

#### V. ASSESSMENT OF PHASE I PROGRAM AND RECOMMENDATIONS FOR PHASE II-EFFORT

##### 1. Assessment of Phase I Program

It has been demonstrated that rms fluctuating pressure and power spectra can be predicted for attached and separated turbulent boundary layer flow. The prediction capability is based on physical laws governing boundary layer flow and shock physics. As a result, the prediction capability allows for scaling parameters that can be used to extrapolate ground test results to flight

conditions. The techniques emphasize the use of attached approach flow conditions, which are tractable, for interaction prediction (i.e., shock/boundary layer) where local flow properties are difficult to determine.

Since supersonic/hypersonic structures require efficient aerodynamic designs, thin surfaces which generate weak shock interactions are generally used. The exceptions to this finding include:

- Corner flow (inlet, stabilizers, and flow guide rails)
- Bow shock interaction (inlet and stabilizer)
- Shock/shock/boundary layer interactions (cowl-inlet, bow-inlet, and bow-cowl-inlet)

Other phenomena that will require investigation include

- Axial-offset interaction relative to boundary layer scale length
- Shock interaction with laminar boundary layers
- Angle-of-attack effects
- Viscous approach flow along the ramp leading to the inlet

A re-examination of aeroacoustic measurements obtained on a cone/slice/flap model at Mach 4 and Mach 8 (AEDC Tunnels A and B) showed that flow separation apparently did not occur. This result was surprising considering flap angles to  $20^\circ$  and angles of attack to  $14^\circ$ . An assessment of these data showed that the small approach flow boundary layer thicknesses and compressibility tended to position the sonic line very close to the surface which would restrict the ability for the flow to separate or render the separation zone to a small region at the compression corner. Other fluid-dynamic phenomena that could impede the separation process include potential wave suppression by expansion waves (cone/slice)

on the compression wave from the slice/flap corner, and the effect of 3D pressure relief occurring during the flow expansion through the cone/slice/flap region. This characteristic would be further realized at angle of attack conditions. Some of these features could be used in the design process to mitigate the impact of flow interaction regions. Finally, the occurrence of transitional flow and entropy (vortical producing flow) have been shown to enhance dynamic pressure to appreciable levels.

## 2. Recommendations for Phase II-Effort

Based on the findings of the Phase I investigation, it was determined that a reasonable data base exists for aeroacoustic loads in attached turbulent boundary layer flows. On the other hand, data for flows featuring shock/boundary layer interactions have been primarily obtained at  $M \leq 3$ . While experiments have been performed at higher Mach numbers, these acoustic data are rendered more useful for fundamental turbulence studies than for the design process. Accordingly, an experimental program is recommended as outlined in the text of this report. The experiments should be conducted in a facility that allows for an interpretation of the interaction process. This will necessitate several preliminary tests to ensure correctness of gage location and flow diagnostic techniques. For this reason, the facilities at WRDC are recommended; in particular the Mach 3 and Mach 12 tunnels which have been extensively characterized and have been used for aeroacoustic testing. This test program will serve to add to the data base that is required for the development of prediction capability and validation of exiting state-of-the-art techniques.



## VI REFERENCES

1. Laganelli, A. L., Martellucci, A. and Shaw, L., "Wall Pressure Fluctuations in Attached Boundary Layer Flow", AIAA Journal V.21, N.4, April 1983 (also AFFDL-TR-77-59).
2. Laganelli, A. L., "Prediction of the Pressure Fluctuations on Maneuvering Reentry Weapons", AFWAL-TR-83-3133, February 1984.
3. Laganelli, A. L., Wolfe, H. F., "Prediction of Fluctuating Pressure in Attached and Separated Turbulent Boundary Layer Flow", AIAA Paper 89-1064.
4. Lilley, G. M., "A Review of Pressure Fluctuations in Turbulent Boundary Layers at Subsonic and Supersonic Speeds", Arch. Mech. Stosow. No. 16, 1964, p. 301.
5. Lowson, M. V., "Prediction of Boundary Layer Pressure Fluctuations", AFFDL-TR-67-167, April 1968.
6. Laganelli, A. L. and Howe, J. R., "Prediction of Pressure Fluctuations Associated with Maneuvering Reentry Weapons", Flight Dynamics Laboratory, Wright-Patterson AFB, AFFDL-TR77-59, July 1977.
7. Laganelli, A. L., Martellucci, A. and Shaw, L., "Predictions of Surface Pressure Fluctuations in Hypersonic Turbulent Boundary Layers", AIAA Paper 76-409, July 1976.
8. Dolling, D.S. and Dussauge, J. P., "Fluctuating Wall Pressure Measurements," Agardograph, 1988.
9. Houbolt, J. C., "On the Estimation of Pressure Fluctuations in Boundary Layers and Wakes" GE TIS 66SD296, April 1966.

10. Robertson, J. E., "Prediction of In-Flight Fluctuating Pressure Environments Including Protuberance Induced Flow", Wyle Laboratories Report WR 71-10, March 1971.
11. Robertson, J. E., "Preliminary Estimates of Space Shuttle Fluctuating Pressure Environments", Wyle Laboratories Report NR 72-10, August 1972.
12. Laganelli, A. L. and Scaggs, N. E., "Wall-shear Characteristics on Smooth and Rough Surfaces Based on Acoustic Measurements", AFWAL TR-85-3114, January 1986.
13. Dolling, D. S., and Or, C.T., "Unsteadiness of the Shock Wave Structure in Attached and Separated Compression Ramp Flowfields", Experiments in Fluids, Vol. 3, 1985, pp. 24-32.
14. Dolling, D. S. and Murphy, M. T., "Unsteadiness of the Separation Shock Wave Structure in a Supersonic Compression Ramp Flowfield", AIAA J., Vol. 21, pp. 1628-1634, December 1983.
15. Muck, K. C., Dussauge, J. P. and Bogdonoff, S. M. "Structure of the Wall Pressure Fluctuations in a Shock-Induced Separated Turbulent Flow", AIAA Paper 85-0179, 23rd Aero Sci. Reno, January 1985.
16. Tan, D. K., Tran, T. T., and Bogdonoff, S. M., "Wall Pressure Fluctuations in a 3-D Shock-Wave/Turbulent Boundary Layer Interaction", AIAA J. V. 25 N. 1, January 1987.
17. Tran, T. T., "Experimental Investigation of Unsteadiness in Swept Shock/Wave/Turbulent Boundary Layer Interactions", PhD Thesis, Princeton University, ME Department, March 1987.

18. Tran, T. T. and Bogdonoff, S. M., "A Study of Unsteadiness of Shock Wave/Turbulent Boundary Layer Interactions from Fluctuating Wall Pressure Measurements", AIAA Paper 87-0552, 25th Aero. Soc., Reno, January 1987.
19. Tan, D. K., Tran, T.T., and Bogdonoff, S. M., "Wall Pressure Fluctuations in a 3-D Shock Wave/Turbulent Boundary Layer Interaction", AIAA J., V. 25, N. 1, January 1987.
20. Tan, D. K., Tran, T. T., and Bogdonoff, S. M., "Surface Pressure Fluctuations in a Three Dimensional Shock Wave Turbulent Boundary Layer Interaction at Various Shock Strengths", AIAA Paper 85-1562 July 1985.
21. Coe, C. F., Chyu, W. J., and Dods, J. B., "Pressure Fluctuations Underlying Attached and Separated Supersonic Turbulent Boundary Layers and Shock Waves," Presented at Aeroacoustic Conference, Seattle, Washington, October 1973, Paper No. 73-996.
22. Laganeili, A., "Prediction of Aeroacoustic Loads for Attached and Separated Turbulent Boundary Layer Flows", SAI Report 89-1052, Final Report to Rohr Industries, Inc., 1989.
23. Krawczyk, W. J. et al., "Computational Models for the Analysis/Design of Hypersonic Scramjet Components - Part II: Inlet and Ramp/Forebody Models", AIAA 86-1596, 22nd Propulsion Conference, July 1986.
24. Krawczyk, W. J., and Harris T. B., "Analysis of Aerospace Vehicle Scramjet Propulsive Flow Fields: 2-D Forebody/Inlet code Development - Phase I", NASP CR-1003, June 1987 (NASP/JPO).

25. Zhen-Hua, S., Smith, D. R., and Smits, A. J. "Wall Pressure Fluctuations in the Reattachment Region of a Supersonic Free Shear Layer" AIAA Paper 90-1461, June 1990.
26. Erengil, M. E. and Dolling D. S. "Correlation of Separation Shock in a Compression Ramp Interaction with Pressure Fluctuations in the Incoming Boundary Layer" AIAA Paper 90-1646, June 1990.
27. Venkateswaran, S., Witte, D. W., and Hunt, L. R., "Aerothermal Study in an Axial Compression Corner with Shock Impingement at Mach 6", AIAA Paper 91-0527, January 1991.
28. Acoustic Loads and Response Workshop for NASP - Held at Pratt and Whitney, West Palm Beach, FL, January 24 and 25, 1991.
29. Krawczyk, W.J., "Analysis of Aerospace Vehicle Scramjet Propulsive Flow Fields: 3-D Forebody Code Development" NASP Contract Report 1029, November 1988.
30. Settles, G. S. and Dolling, D. S., "Swept Shock Wave/Boundary Layer Interactions," Tactical Missile Aerodynamics, Progress in Astronautics-Aeronautics (AIAA) V 104.
31. Inger, G. R., "Spanwise Propagation of Upstream Influence in Conical Swept Shock/Boundary Interactions", AIAA J., V. 25, N. 2, February 1987.
32. Inger, G. R., - Private Communication (Science Applications International Corporation Consultant - Iowa State University) December 1988.